Digital Discovery

ROYAL SOCIETY OF CHEMISTRY

REVIEW

View Article Online
View Journal | View Issue

Cite this: *Digital Discovery*, 2025, **4**, 2364

Flow chemistry as a tool for high throughput experimentation

George Lyall-Brookes, Alex C. Padgham and Anna G. Slater *

Received 31st March 2025
Accepted 13th July 2025

DOI: 10.1039/d5dd00129c

rsc.li/digitaldiscovery

The way in which compounds and processes are discovered, screened, and optimised is changing, catalysed *via* the advancement of technology and automation. High throughput experimentation (HTE) is one of the most prevalent techniques in this area, with applications found across a broad spectrum of chemical fields. However, limitations such as challenges in handling volatile solvents mean it is not suitable for all applications, and scale-up can require extensive re-optimisation from an initial high throughput screening (HTS). These challenges can be addressed by coupling HTS with other enabling technologies, such as flow chemistry. The use of flow also widens available process windows, giving access to chemistry that is extremely challenging to carry out under batch-wise HTS. This review will highlight key contributions of flow chemistry approaches for HTS across six research areas, outlining applications, capabilities and benefits, finishing with comments on future directions for the technology.

Introduction

Historically, the discovery and development of reactions has relied upon the creativity and persistence of chemists, paving the way for modern advancements. Often, major breakthroughs have been attributed to serendipity and unexpected outcomes, but societal pressures have led researchers to seek more efficient methods to accelerate innovation.[1] As such, the chemical community has increasingly turned to enabling technologies to facilitate the move away from trial-and-error, one reaction at a time approaches;[2] these new platforms allow workflows that reduce the time required to develop synthetic methodologies, *via* improved optimisation capabilities and a simplified translation to desired larger scale processes.

Flow chemistry is one of the enabling technologies used to enable more efficient reaction screening.[3] The technique is well-established for large-scale manufacturing in the oil, gas and petroleum industries,[4] with the first references to the use of a 'flow reactor' dating back to the 1930s.[5] However, it is only within the last two decades that interest for the technology has grown within the chemical community,[6] primarily stemming from the ability to improve chemical processes that are inefficient and challenging to control under batch conditions.[7]

Department of Chemistry and Materials Innovation Factory, University of Liverpool, Liverpool L69 7ZD, UK. E-mail: anna.slater@liverpool.ac.uk

George Lyall-Brookes

George Lyall-Brookes completed his master's degree at Durham University in 2022 under the supervision of Prof. Ian Baxendale, working on the synthesis of functionalised nitrobenzene derivatives using flow chemistry. George then joined Sterling Pharma Solutions as a Flow Chemistry Development Chemist, before pursuing a PhD at the University of Liverpool. He is currently a doctoral student under the supervision of Anna Slater and Prudence Wong, focusing on the use of self-optimising algorithms in the synthesis of organic compounds and materials in flow.

Alex C. Padgham

Dr Alex C. Padgham completed his MChem with a Year in Industry (GSK) at the University of Sussex (2011) and graduated from Imperial College London with a PhD in Organic Chemistry (2018), working on novel methodologies with Prof. Philip Parsons. His first PDRA position was in the group of Dr Marcus Baumann at University College Dublin where, in collaboration with Pfizer Ireland, the use of flow chemistry in API synthesis was investigated. Currently he is working as a PDRA in the Slater group, exploring the use of new and continuous technologies in organic and supramolecular chemistry.

Compared to batch conditions, flow chemistry can provide benefits due to the improved heat and mass transfer afforded through the use of narrow tubing and/or chip reactors: the so-called miniaturisation.[8] The low volume of reactive material, at any one time, allows the safe use of hazardous and explosive reagents[9] such as alkyl lithium,[10] azides[11–14] and diazo containing compounds.[15,16] The ease of pressurising flow systems enables the use of solvents at temperatures far in excess of their boiling points under atmospheric pressure, offering wide process windows and accelerated reaction rates. Finally, the precise control of reaction time and temperature, and accessible in flow, decrease the risk of undesired side- and by-products, as well as decomposition.[17]

Flow chemistry has further been beneficial in the development of novel methods of automation; fully automated flow chemistry platforms can now be found within the literature,[18–20] as well as being commercially available.[21–24] Such platforms have further expanded the scope of what flow chemistry systems can achieve, with applications including synthesis,[25,26] autonomous optimisation,[27,28] kinetic studies[29–31] and, most pertinent to this review, reaction screening.[3,32] However, flow chemistry is not typically carried out in parallel; although throughput of an individual reaction can be dramatically increased *via* process intensification in flow, the technique is generally not thought of as suitable for screening many reactions or substrates simultaneously.

Here, a complementary powerful method of conducting reaction screening is with high throughput experimentation (HTE),[33,34] where a wide chemical reaction space is explored by employing diverse conditions for a given synthesis or transformation, typically determined by the literature, past experience, or scientific intuition.[35] This allows reactions to be conducted in parallel on a large scale in a 'brute force' approach, drastically reducing the time required to conduct a comparable number of experiments in a traditional manner:[36] for example, the time taken to conduct screening of 3000 compounds against a therapeutic target could be reduced from 1–2 years to 3–4 weeks.[37] Automation of reaction screening stems from the life sciences, where it has a long history,[38–40] and in which it is now widely prevalent, primarily for microscopy-based functional analysis screens, using 96- and 384-well plates with typical well volumes of ~300 μL.[41]

Initially, chemists adopted a similar approach to biologists, *i.e.*, conducting reactions in parallel in ~300 μL, 96- or greater microwell plates, used in conjunction with additional mixing and cooling components as needed. Plate-based approaches are still prevalent within many chemical disciplines due to their relatively straightforward operation. However, the use of plates in HTE can bring limitations: for example, continuous variables such as temperature, pressure and reaction time are challenging to investigate.[42] Optimised parameters identified *via* plate-based screening also often require re-optimisation when reaction scale is increased, negating the time-saving benefits of HTS. As such, alternative approaches have been explored, with the combination of flow chemistry and HTE proving particularly fruitful.

In flow, the continuous variables of a process may be dynamically altered throughout the duration of an experiment;[43] this presents an opportunity to investigate and manipulate such variables in a high-throughput manner, in a way not possible in batch. Similarly, the use of flow means scale can be increased by increasing operating time, affording access to tractable quantities of substrates without changing the process. It is also easier to maintain the heat and mass transfer of the process in flow across reactor scales compared to batch, reducing re-optimisation requirements. The wide process windows and improved safety profiles of flow chemistry mean that HTE can now be conducted within chemical laboratories on "challenging" and hazardous chemistry, and at increasingly larger scales. Finally, the advancement and automation of analytical techniques in flow, including inline/real-time process analytical technologies (PAT), have enabled more efficient HTE workflows requiring less material and human intervention,[44] leading to widespread adoption across various chemical disciplines,[45] within both industrial[44,46–48] and academic settings.[49–51]

Herein we will outline the use of flow chemistry in HTE across six key research areas: photochemistry, algorithmic optimisation, catalysis, electrochemistry, medicinal chemistry and material/supramolecular chemistry. Key examples illustrating the impact of the technology will be used to highlight the applications and benefits of combining these complementary techniques, and to suggest future directions for development.

Anna G. Slater

Prof. Anna Slater received her PhD on the synthesis and surface self-assembly of perylene diimide derivatives from the University of Nottingham in 2011, working with Prof. Neil Champness. Following PDRA positions in porphyrin synthesis and functional organic materials, the latter in the group of Prof. Andew Cooper, she was awarded a Royal Society-EPSRC Dorothy Hodgkin Fellowship to begin her independent career in 2016. She is now working as a Royal Society University Research Fellow and Professor of Chemistry at the University of Liverpool's Materials Innovation Factory. Her current research interests focus on the development of innovative tools for the discovery, optimisation, scale-up, and translation of functional organic and supramolecular materials.

Flow HTE in photochemistry

One of the most prevalent areas where HTS is combined with flow is for photochemical reactions. Flow chemistry lends itself well to photochemical transformations that are challenging for traditional batch chemistry; in batch, poor light penetration and non-uniform irradiation leads to poor selectivities and conversions, particularly at larger scales. The use of flow reactors can enable efficient photochemical processes *via*

minimising the light path length and precisely controlling irradiation time.[52–55] Many examples of commercial[56–59] and bespoke[60–62] photochemical reactors exist within the literature and have been implemented with great success. Despite this, determining the optimal conditions for a photochemical process can often prove challenging and time consuming, and as such HTE is becoming increasingly popular to expedite this task, particularly within the pharmaceutical industry.

The most commonly employed approach for HTE screening of photochemical parameters is through the use of 24–96 multi-well batch photoreactors.[63–70] Jerkovic *et al.* used this approach in the development and scale up of a flavin-catalysed photoredox fluorodecarboxylation reaction (Fig. 1a).[71] 24 photocatalysts, 13 bases, and 4 fluorinating agents were selected based on existing literature and screened across four HTE experiments using a 96 well plate-based reactor, with the solvent composition, scale and light wavelength kept consistent. The screening returned several hits outside of the previously reported optimal conditions, with two optimal photocatalysts and bases identified in addition to the best fluorinating agent. These hits were then validated using a batch reactor[72] and optimised using a design of experiments (DoE) approach.[73]

Due to the heterogeneous nature of the batch optimised procedure, further photocatalyst screening was conducted in an attempt to develop a homogeneous procedure, to negate the risk of clogging or fouling in a flow reactor. A homogeneous, and equally effective, photocatalyst was identified and used moving forward – an additional DoE study was also conducted to further optimise the new conditions. Time-course ^{1}H NMR data were also collected to optimise residence time, and a stability study of the reaction components was conducted to determine the composition and number of feed solutions required. The process was initially transferred to flow on a small scale using a Vapourtec Ltd UV150 photoreactor;[57] returning a conversion of 95% on a 2 g scale. Gradual scale up and optimisation of flow reaction parameters (*i.e.*, light power intensity, residence time and water bath temperature) were subsequently conducted using a "custom" two-feed set up (Fig. 1b), achieving a 100 g scale. Finally, the optimal conditions were carried through to the kilo scale where 1.23 kg of the desired product was obtained at a conversion of 97% and a yield of 92%, corresponding to a throughput of 6.56 kg per day.

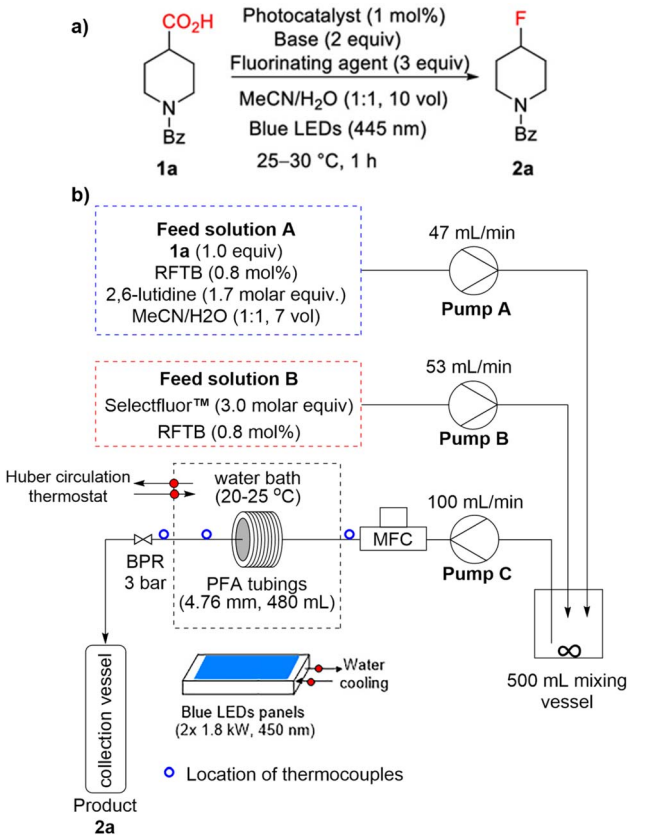

Fig. 1 (a) Flavin-catalysed photoredox fluorodecarboxylation reaction, (b) schematic diagram of the setup employed using a two-feed approach – adapted with permission from Jerkovic *et al.*[71] Copyright © 2024 American Chemical Society.

Mori *et al.* reported a comparable approach to investigate cross-electrophile coupling of strained heterocycles with aryl bromides (Scheme 1),[74] employing a 384-well microtiter plate photoreactor to identify the optimal conditions for the reaction of interest. Following this initial screening, further optimisation of the reaction parameters was conducted in a smaller 96-well microtiter plate reactor, expanding the scope and achieving conversions of up to 84%. The 96-well plate was then used once again, in three batches of reactions, for the synthesis of 110 compounds, with the final products purified *via* preparative liquid chromatography-mass spectrometry (LC-MS), forming a library of drug-like compounds.

Following determination of the optimal coupling conditions, a small parameter study was conducted to elucidate the optimal flow conditions for the reaction, with the highest yield achieved at 60 °C and a 10-minute residence time. These optimised conditions were then subsequently adapted to the gram scale synthesis of a targeted compound, using a commercially available automated synthesiser, capable of synthesising multiple small-volume samples. Used in conjunction with an in-house developed photoreactor, 1.3 g of the material could be synthesised from a 2.5 hour run time with a residence time of 15 minutes in the photoreactor.

Despite the success of these approaches, they highlight a significant limitation of the use of batch HTE equipment: that optimal parameters cannot be directly translated to flow to enable the scale up of the process, and that additional resources and time allocation are required.[75] To avoid this issue, González-Esguevillas *et al.* adjusted the solution level used within a standard 96-well plate to match the exact internal diameter of a flow reactor, ensuring that the path length of the light remained constant across both batch and flow (Fig. 2a) and reducing the need for re-optimisation.[51] To further facilitate comparable light exposure to a flow reactor coil element, a glass 96-well plate platform was developed ("FLOSIM"), which used LEDs and concave lenses/high density reflection mirrors to achieve uniform photon dispersion (Fig. 2b). The FLOSIM platform was validated *via* the optimisation of a variety of photoredox reactions. The workflow consisted of an initial

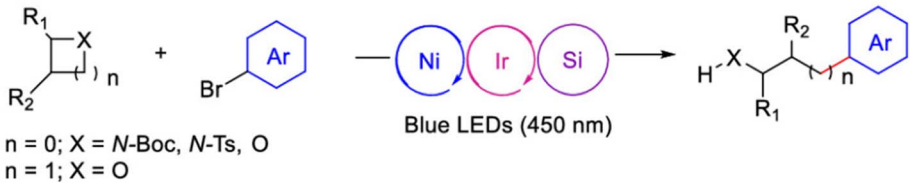

Scheme 1 Photoredox-assisted reductive cross-coupling reaction of strained aliphatic heterocycles with aryl bromide – reproduced from Mori *et al.*[74] with permission. Copyright © 2023 American Chemical Society.

validation of the reaction in batch across various wavelengths, followed by screening the conditions on the FLOSIM platform using light source exposure times equivalent to the desired residence time in flow. The identified optimised parameters were then directly transferred to a commercially available Vapourtec E-series UV-150 system for scale up (Fig. 2c).

A further challenge for batch HTS photochemistry is reproducibility issues arising from differences in irradiation between

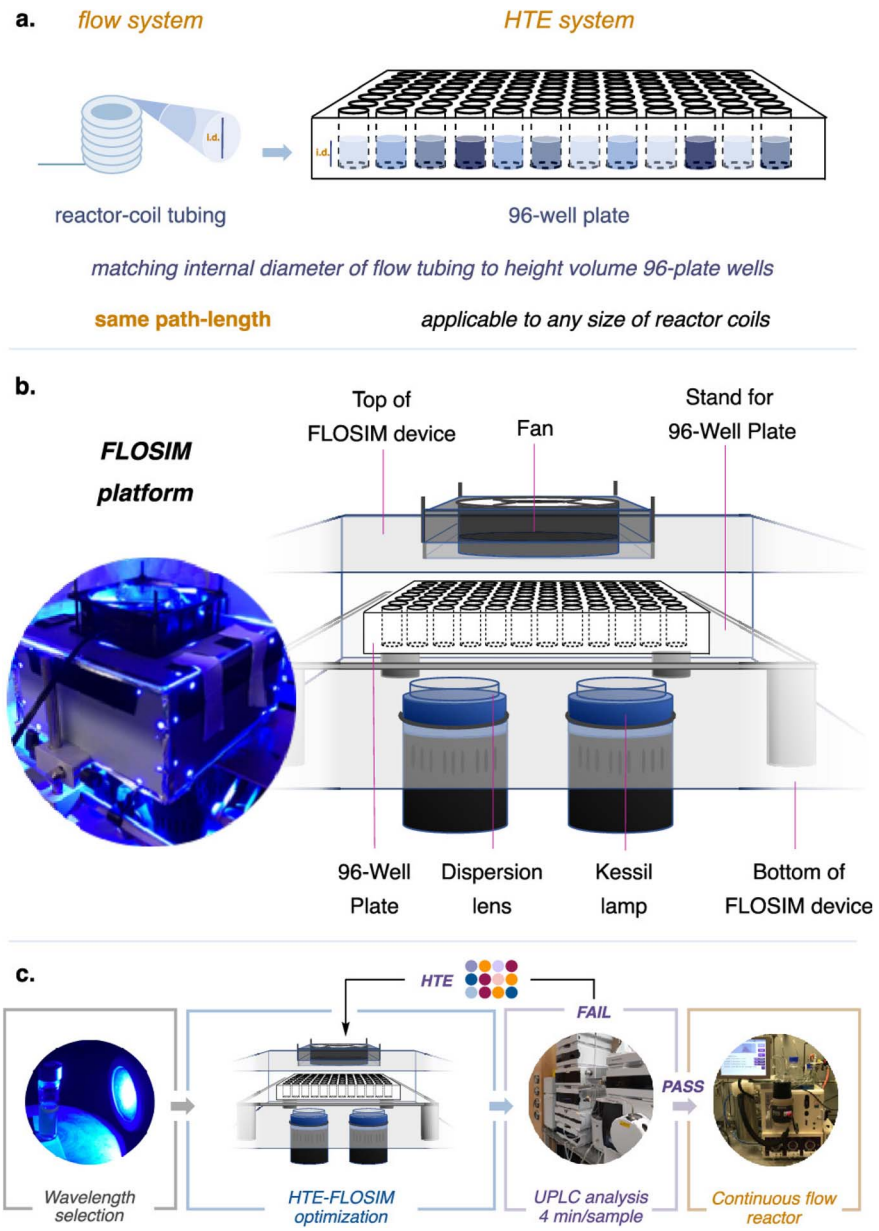

Fig. 2 (a) Well-plate to flow translation concept, (b) FLOSIM platform for well-plate to flow translation, and (c) outlined workflow for optimisation of photoredox reactions – reproduced from González-Esguevillas *et al.*[51] with permission under the Creative Commons Attribution license (CC-BY-NC-ND 4.0). Copyright © 2021, González-Esguevillas *et al.*

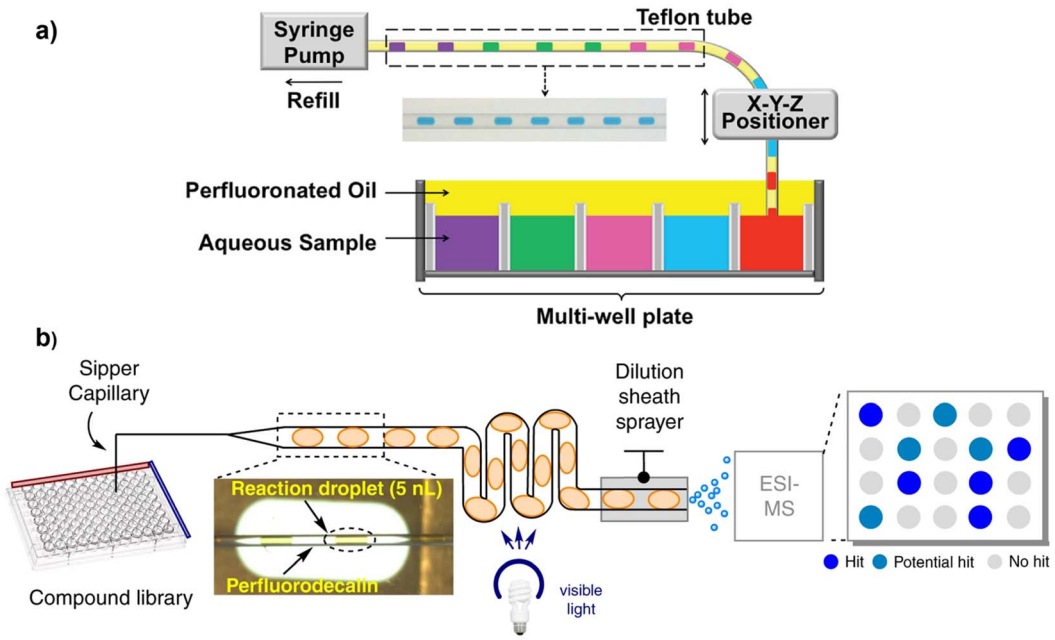

Fig. 3 (a) Diagram of oil-segmented droplet generation from a micro-well plate – reprinted with permission from Sun *et al.*[86] Copyright © 2020 American Chemical Society and (b) photochemical droplet microfluidic platform – reproduced from Sun *et al.*[75] with permission under the Creative Commons Attribution license (CC-BY). Copyright © 2020, Sun *et al.*

different wells and in different reactors, as noted by Pijper *et al.*[76] To avoid this, slug-flow continuous approaches, where segments of material are separated by an immiscible fluid or gas,[77] have been developed as an alternative HTS strategy.[18,75,78–82] Use of slug- or droplet-flow methods also minimises the amount of material consumed during screening, as reactions are typically conducted on the nanolitre to femtolitre scale, an up to eightfold reduction in starting material consumption in comparison to traditional plate-based screening.[76] Such platforms also avoid the pitfalls of traditional screening platforms, as volatile solvents can be used without evaporation, broad operating windows can be applied and continuous variables can be easily adjusted.[83] The principles of such platforms have been discussed in a previous review,[84] with Arshad *et al.*[83] and Yu *et al.*[45] discussing the use cases of such platforms.

An example of a slug-flow platform being used for HTE can be seen in the screening of visible light-driven trifluoromethylation reactions,[75] first reported by Beatty *et al.* (Fig. 3b).[85] The platform incorporated droplet microfluidics and electrospray ionization-mass spectrometry (ESI-MS) analysis to facilitate high throughput reaction discovery in flow. Droplet samples (5–10 nL) were aspirated from standard 384 or 1536 microwell plates[86–89] and segmented by using a perfluorodecalin carrier (8 nL) in 100 μm internal diameter perfluoroalkoxy alkyl tubing (Fig. 3a). The samples were then irradiated for 10 minutes *via* a visible-light source and transported to a sheath sprayer for in-line dilution. The dilution served the dual purpose of quenching the reaction and diluting the sample to a suitable detection range for the MS analysis.

Following the initial success of a small-scale preliminary investigation into a platform capable of carrying out the radical trifluoromethylation reaction, Sun *et al.* further developed the platform to generate a library of alkene aminoarylation products. An oscillating flow system was induced *via* use of a syringe pump operated in withdrawal and infusion modes (Fig. 4). The use of an oscillating flow system enables prolonged irradiation of the droplets whilst maintaining a constant flow. The syringe pump was used in conjunction with a custom-built Cree LED array photoreactor[88] in order to maximise photon flux, a metric describing the number of photons per second per unit area. 100–200 droplets could be irradiated per incubation period, more than 100 times greater than comparative state-of-the-art oscillating flow systems.[90,91] ESI-MS analysis was used to confirm product formation at a throughput of 0.3 samples per second, with a total of 350 sampled within a 19-minute window.

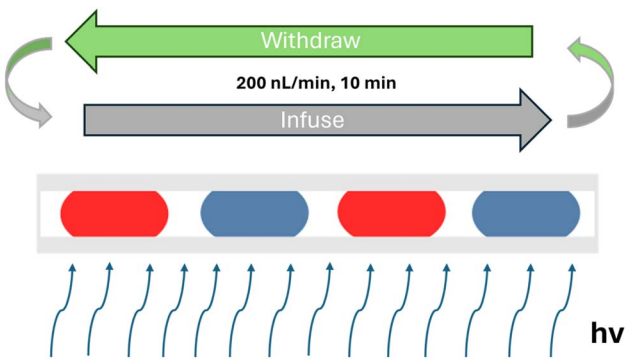

Fig. 4 Schematic representation of an oscillating flow reactor whilst being irradiated – reproduced from Sun *et al.*[75] with permission under the Creative Commons Attribution license (CC-BY). Copyright © 2020, Sun *et al.*

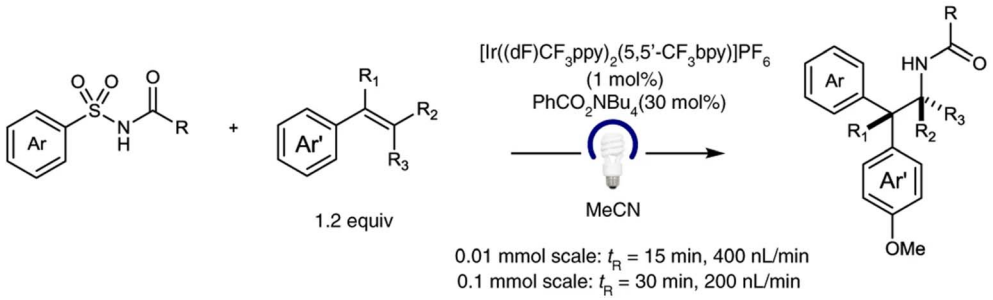

Scheme 2 Alkene aminoarylation formation reaction investigation – reproduced from Sun *et al.*[75] with permission under the Creative Commons Attribution license (CC-BY). Copyright © 2020, Sun *et al.*

Ten sulfonylacetamides and ten alkenes were selected for screening (Scheme 2); of the potential 100 product combinations, 37 hit conditions were identified, with nine of the droplet reactions selected to validate the platform on the 0.01 mmol scale. Seven of these were successful, with the two unvalidated reactions attributed to initial false hits due to byproducts with the same *m*/*z* signal as the desired products. Translatability of the platform to a microscale flow reaction was then investigated at a 0.1 mmol scale to generate material on a milligram scale, as needed for discovery chemistry applications. The same nine reactions were scaled up and isolated, with comparable yields to the previously conducted 0.01 mmol scale reactions.

Further work by Sun *et al.* incorporated nanoelectrospray-ionisation mass spectrometry (nESI-MS) analysis into the workflow (Fig. 5),[78] increasing throughput to 2.9 samples per second, a near 10 fold increase.[75] The platform was used to screen photoredox catalysis in a plate-based format, with samples transferred *via* segmented droplet flow for nESI-MS analysis. A benchtop modular photoreactor was designed for irradiation of the microwell plate reactions using high power LEDs in a 25 LED array to accommodate standard 96, 384 or 1536 well plates. Premixed reaction solutions were irradiated in the microwell plate, followed by withdrawal and dilution of an aliquot of the reaction solution. 8 μL of the subsequent solution was then transferred to a separate well for droplet formation, as per the previously developed workflow.[75]

The workflow was validated using radical perfluoroalkylation reactions developed by the Stephenson group,[85,92,93] specifically the photoredox trifluoromethylation of *N*-Boc-5-bromo-7-azaindole and caffeine (Fig. 6a). Product formation could be tracked successfully for the two reactions. Following validation, the strategy was used in the late stage fluoroalkylation (CF_3, CF_2H, and CF_2Cl) of drug like compounds (Fig. 6b), high throughput optimisation of photoredox reaction conditions (Fig. 6c) and the late-stage functionalisation of a compound library for subsequent biological screening (Fig. 6d). A throughput of 0.67 droplets per second was used in each case, although this could be increased to 2.9 droplets per second, decreasing the time needed for a 384 microwell plate to under 7 minutes compared to the 422 minutes that the same work would require *via* LC-MS analysis.[44]

As shown by these examples, high-throughput droplet screening can vastly increase the efficiency of reaction screening, especially when combined with advanced analytical techniques as in the studies above. However, the utility of such approaches is not solely limited to photochemistry: combining the advantages of real-time, inline analysis with automated data-processing provides opportunities to further increase efficiency of chemical reaction discovery and for development *via* autonomous optimisation strategies.

Flow HTE to enhance algorithmic optimisation

Time- and resource-intensive optimisation problems are increasingly being taken out of the hands of chemists, for example *via* the use of self-optimising systems rather than one factor at a time (OFAT) approaches. Self-optimising systems use inline analytical data to autonomously derive the next set of experimental conditions, typically *via* the use of machine learning algorithms, forming a closed loop optimisation cycle.[94] The cycle is repeated iteratively until a predetermined or

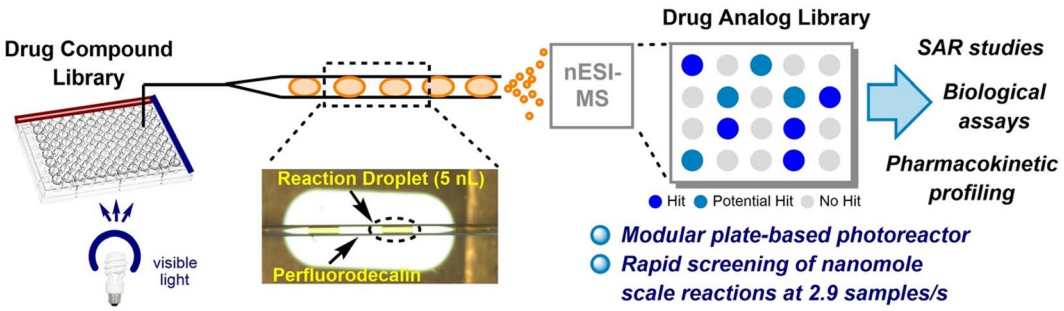

Fig. 5 Overview of a droplet nESI-MS platform for screening plate-based photochemical reactions – reproduced from Sun *et al.*[78] with permission under the Creative Commons Attribution license (CC-BY-NC). Copyright © 2023, Sun *et al.*

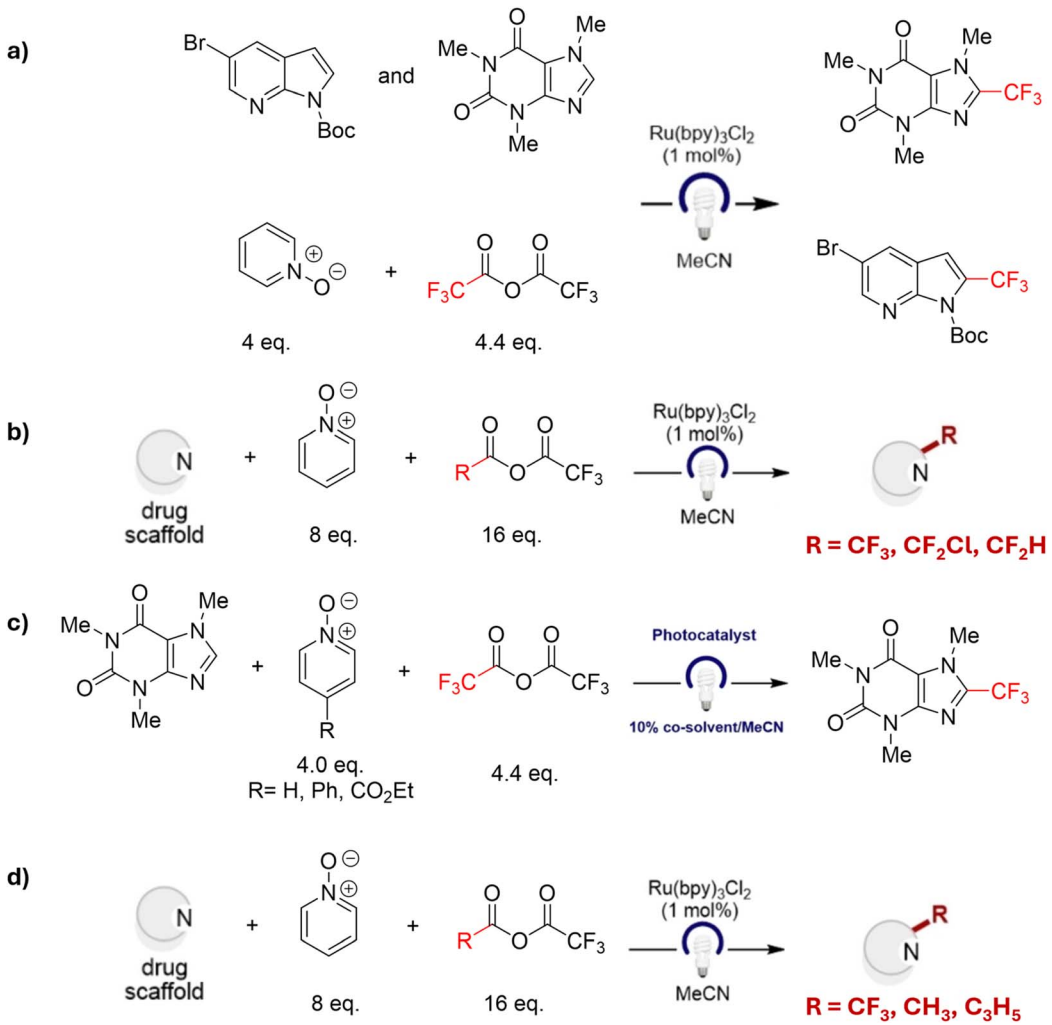

Fig. 6 (a) Photoredox trifluoromethylation of caffeine and 5-Br-7-(*N*-Boc)azaindole substrates, (b) late stage fluoroalkylation (CF_3, CF_2H, and CF_2Cl) of drug like compounds, (c) high throughput optimisation of photoredox reaction conditions, and (d) late-stage functionalisation of a compound library for subsequent biological screening. Reproduced from Sun *et al.*[78] with permission under the Creative Commons Attribution license (CC-BY-NC). Copyright © 2023, Sun *et al.*

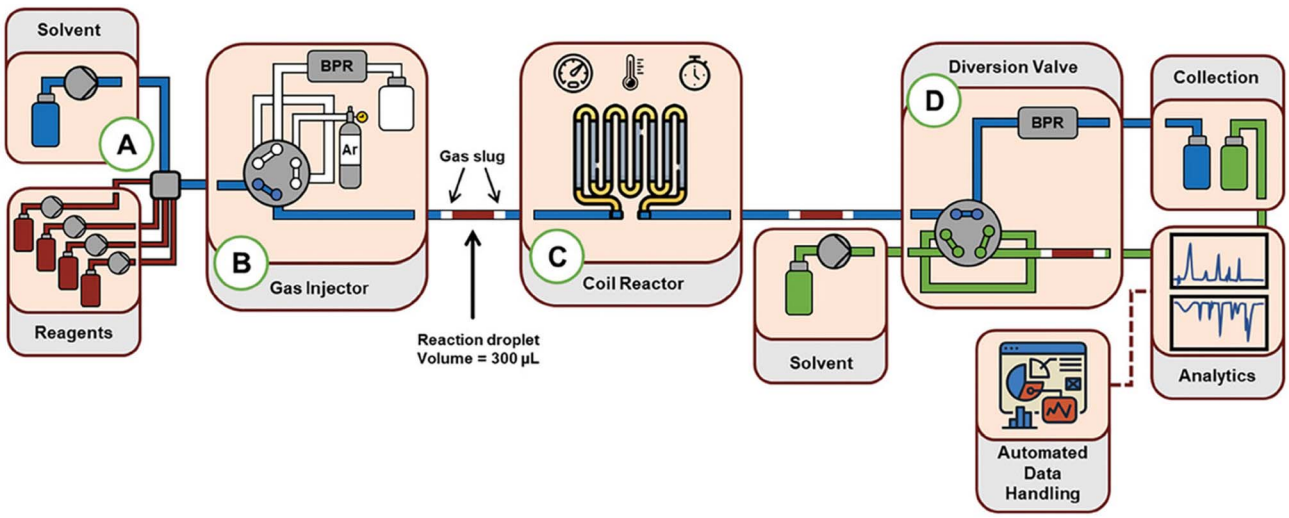

Fig. 7 Schematic representation of the reactor platform employed. (A) Reagent and solvent pumps, combined in a 6-way mixer. (B) Sample loop for gas injection. (C) Heated coil reactor. (D) 6-Port valve to direct the reaction slug for analysis – reproduced from Wagner *et al.*[77] with permission under the Creative Commons Attribution license (CC-BY 4.0). Copyright © 2024, Wagner *et al.*

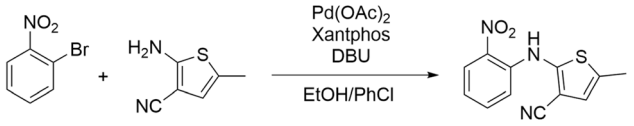

Scheme 3 Buchwald–Hartwig reaction investigated by Wagner *et al.*[77] adapted from Wagner *et al.*[77] with permission under the Creative Commons Attribution license (CC-BY 4.0). Copyright © 2024, Wagner *et al.*

maximum value for the optimisation variable is reached, or after a pre-set number of cycles.

Flow chemistry lends itself particularly well to this approach due to the iterative nature of conducting individual flow reactions,[95] the nature of inline analysis *via* PAT, and the improved process control that ensures that data points are accurate and repeatable. Initially, self-optimising systems were used to maximise a singular variable such as yield or conversions; however, as algorithms have advanced, multiple variables can now be optimised simultaneously accounting for trade-offs between the variables.[96]

Wagner *et al.* reported the development of a self-optimising system for reaction optimisation that employed a slug flow regime. The use of 300 μL reaction slugs meant a large number of reaction iterations could be run while consuming ~10% of the material needed for a standard flow experiment and reducing the time taken to reach the global optimum.[77] A Fourier transform infrared (FTIR) spectrometer and ultra high-performance liquid chromatograph (UHPLC) were employed synergistically; use of a sample loop ensured that even at different reaction flow rates, the samples were delivered into the flow cell at a constant velocity for consistent analysis. The FTIR recorded a spectrum once every five seconds; once a reaction slug was detected a signal was sent to the UHPLC to inject the sample and begin measuring (Fig. 7). As such, the platform is ideal to explore the efficiency of various optimisation strategies without excessive use of resources or waste generation.

A Buchwald–Hartwig amination reaction (Scheme 3) was selected to validate the set-up due to its mechanistic complexity and numerous potential optimisation variables. Six independent optimisation variables were investigated: amine loading, reaction concentration, residence time, reaction temperature, base loading and catalyst loading. The study used three different optimisation strategies: multi-objective self-optimisation using Bayesian optimisation, DoE and a kinetic study (Fig. 8).

Self-optimisation was executed using the Thompson Sampling Efficient Multi-Objective (TSEMO) Bayesian optimisation algorithm, with broad ranges for the selected optimisation variables: yield (%), space time yield (STY) (kg L^{-1} h^{-1}), and cost (based on solution consumption). 12 Latin hypercube (LHC) sampling experiments were employed,[97] followed by a further 48 iterations guided by Bayesian optimisation, resulting in a total of 60 reactions conducted in ~12 hours and minimal material consumption – only 7% of the theoretical quantity of material required to conduct comparable reactions at a steady state was consumed. A maximum yield of 91% was achieved and, under differing conditions, a maximum STY of 1.13 kg L^{-1} h^{-1} could be obtained. No trends were observed when varying reaction concentration, amine loading, or 1,8-diazabicyclo[5.4.0]undec-7-ene (DBU) loading. A control experimental point was repeated several times to establish reproducibility.

The results of the Bayesian optimisation informed the parameter selection for a DoE study, with residence time and concentration kept constant as a result. A face-centred full factorial design was selected, including 24 experiments and centre points to test reproducibility. Certain parameters, such as temperature and catalyst loading, were intentionally narrowed to ensure that the most relevant area of the design space was explored, whilst other parameters remained relatively flexible. The resulting model for predicting reaction yield provided an excellent fit for the observed reaction yield, returning a R^2 value of 0.904 (Fig. 9), and good reproducibility, with only a 6%

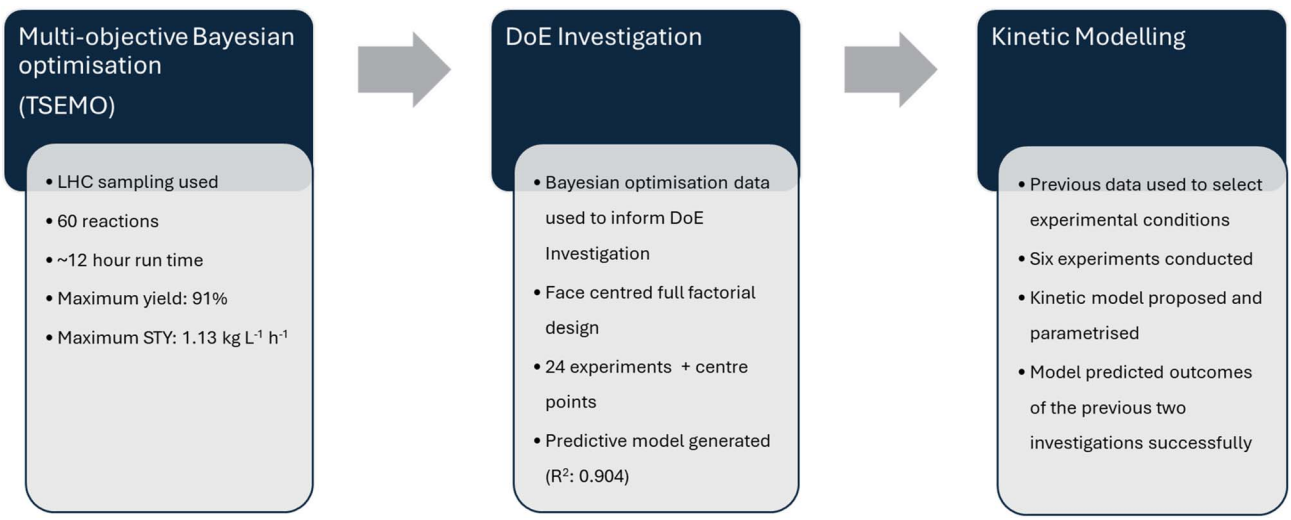

Fig. 8 Process flowchart for the study outlined by Wagner *et al.*[77]

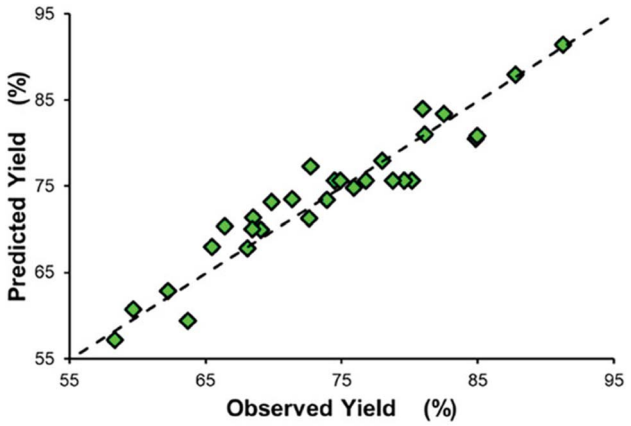

Fig. 9 Predicted results obtained *via* the DoE study *versus* observed results for the reaction yield – reproduced from Wagner *et al.*[77] with permission under the Creative Commons Attribution license (CC-BY 4.0). Copyright © 2024, Wagner *et al.*

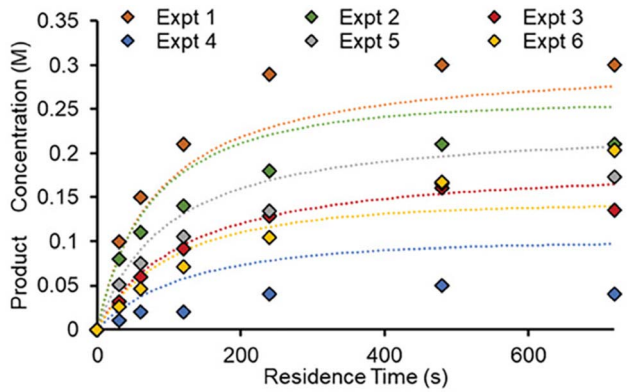

Fig. 10 Plot showing product (5-methyl-2-((2-nitrophenyl)amino) thiophene-3-carbonitrile) concentration across six different time-course experiments. Points denote experimental measurements, whilst dotted lines denote predicted values using the fitted kinetic model – reproduced from Wagner *et al.*[77] with permission under the Creative Commons Attribution license (CC-BY 4.0). Copyright © 2024, Wagner *et al.*

yield disparity observed between replicated runs. DBU loading was found to have a profound effect on the yield of the reaction in direct contrast to the findings of the Bayesian optimisation experiments; it was speculated that this could be a result of the narrower parameter window explored as part of the DoE design.

The third and final experimental design used kinetic modelling of a selection of six experimental conditions, based upon prior data collected in the study, to examine variation in the optimised parameters (Fig. 10). For each of these conditions, six experiments were performed at residence times between 0.5 and 12 minutes, with the resulting data used to propose a kinetic model and define the parameters, which in turn provided the rate of reaction data. The model was able to predict the outcomes for both the self-optimised and DoE experimental results, returning root-mean square error values of 34.9 mM and 25.0 mM respectively (a metric describing the average difference between a value predicted by a model and the actual values). This highlighted the capabilities of the model to provide more accurate predictions within the design space of interest, despite being fitted to a smaller area of the design space.

The use of multiple optimisation strategies allows comparison of their advantages and disadvantages, and to develop appropriate experimental workflows that best fit the optimisation problem at hand. Along these lines, Wagner *et al.* reported a further study using Bayesian optimisation to address the following questions: (1) when to use an exploitation-focused algorithm (exploring chemical space around previously identified points), and when to use an exploration-focused algorithm (targeting wide exploration of previously unexplored regions)? (2) What is the best approach to tackle multi-objective optimisation problems? (3) Can previous knowledge of similar reactions be used to accelerate reaction optimisation?[95]

To answer the first question, an expected improvement (EI) based Bayesian optimisation algorithm, which favours exploitation over exploration, and a single objective implementation of the TSEMO algorithm, which balances both exploration and exploitation, were applied for the optimisation of the amide coupling of benzoic acid and benzylamine (Scheme 4). Both algorithms returned comparable optimum yields, with 77% and 72% observed for the EI and the TSEMO algorithms, respectively; however, the EI algorithm returned that value in six experiments, half the number of the experiments for the TSEMO algorithm, although at the expense of exploration efficiency. Limited improvement to the exploration of the EI algorithm was observed *via* the introduction of LHC sampling across 13 experiments. The authors proposed that by incorporating a 10 experiment LHC sample, the issue could be minimised by providing more knowledge of the design space; this can ensure that a global optimum can be found, albeit at the expense of the experimental budget. The benefits and

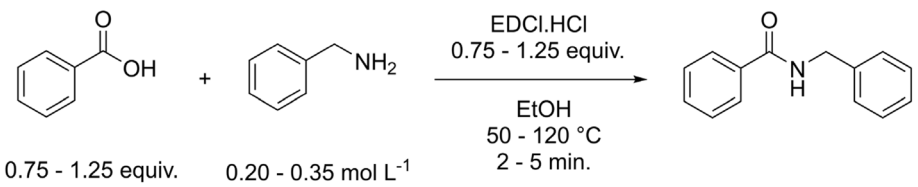

Scheme 4 Amide coupling of benzoic acid and benzylamine with EDCI·HCl (*N*-(3-dimethylaminopropyl)-*N*′-ethylcarbodiimide hydrochloride) and EtOH (ethanol), featuring input parameter boundaries. Adapted from Wagner *et al.*[95] with permission under the Creative Commons Attribution license (CC-BY 4.0). Copyright © 2024, Wagner *et al.*

$$\text{Score} = \frac{\text{weight}_{\text{yield}} \times \text{yield} - \sum\left(\text{excess}_i{}^2 \times \text{weight}_i\right)}{\text{weight}_{\text{yield}}}$$

Scheme 5 The general structure of the weight function applied to the results – reproduced from Wagner *et al.*[95] with permission under the Creative Commons Attribution license (CC-BY 4.0). Copyright © 2024, Wagner *et al.*

limitations of EI based algorithms were displayed in this work: they are best employed when extensive reaction data exist for a given transformation, such that optimal reaction conditions can be found *via* prioritising exploitation; in contrast, multi-objective optimisation algorithms, such as TSEMO, are best employed for reactions with limited available data, where a more complete balance of exploration *vs.* exploration is required.

Upon expanding the variable boundaries, LHC sampling returned yields >90%, although this required the use of large reagent excess, high temperatures and long residence times, meaning the process had poor environmental metrics and throughput. Here the authors address the second query: how to most efficiently approach multi-objective optimisation problems? A weighted approach was adopted,[98] employing user-assigned weights to undesirable inputs, returning a score for each experiment (Scheme 5). The acquired reaction data were compared to a standard multi-objective algorithm in the form of multi-objective TSEMO, *in silico*; the weight function approach outperformed the standard algorithm in the region of interest, mapping a more relevant section of the Pareto front, which is defined as a set of optimal trade-offs between conflicting objectives.[99] Thus the authors concluded that the use of a weighted approach, as opposed to the use of an algorithm such as TSEMO, proved optimal for mapping a relevant section of the Pareto front, when the deemed optimal parameters proved unfavourable from a throughput and environmental perspective.

Finally, Wagner *et al.* set about addressing how existing reaction data can be leveraged in reaction optimisation.[95] To probe this, three variations to the standard reaction conditions were adopted to see whether prior knowledge from the previous campaign could accelerate optimisation for related chemistry: a change in the coupling reagent, a change to an unreactive electron deficient aniline, and a change to both reactants and coupling partners. Successful conditions for the standard reaction (Fig. 11a) were identified, returning a yield of 99% and

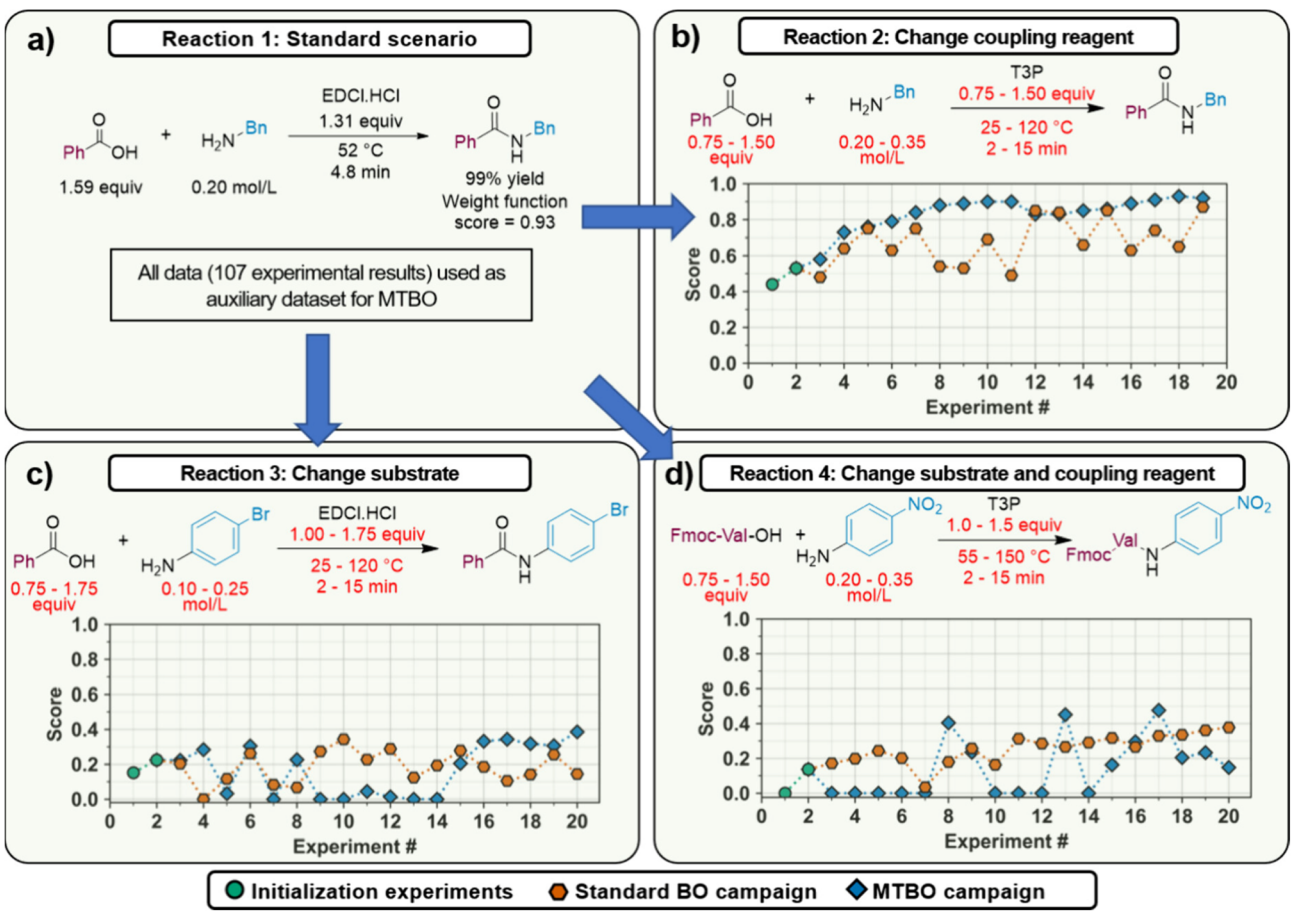

Fig. 11 Summary of attempts to use MTBO to accelerate optimization across different reactions. (a) The standard reaction scenario used for other comparisons in this study, (b) transfer to a different coupling reagent in reaction (2), (c) transfer to a different substrate in reaction (3), and (d) transfer to different substrates and coupling reagents in reaction (4) – reproduced from Wagner *et al.*[95] with permission under the Creative Commons Attribution license (CC-BY 4.0). Copyright © 2024, Wagner *et al.*

0.93 weight function score. A multitask Bayesian optimisation algorithm[100,101] was trained using the reaction data. When the algorithm was applied to a reaction with comparable reactivity (Fig. 11b) to the data set in which it was trained, the algorithm returns excellent results (99% yield, 10 experiments). However, when little overlap existed between the training data set and the reaction intended for optimisation (Fig. 11c and d), the algorithm was less successful, giving results comparable to, or worse than, a standard Bayesian optimisation approach. From this it can be concluded that multi-task algorithms are ill-suited for tasks that differ too far from the auxiliary task in which they are trained (Fig. 11c and d). However, they excel when applied to tasks comparable to the auxiliary task, presenting a particular opportunity for their application in the generation of compound libraries with comparable structural motifs and

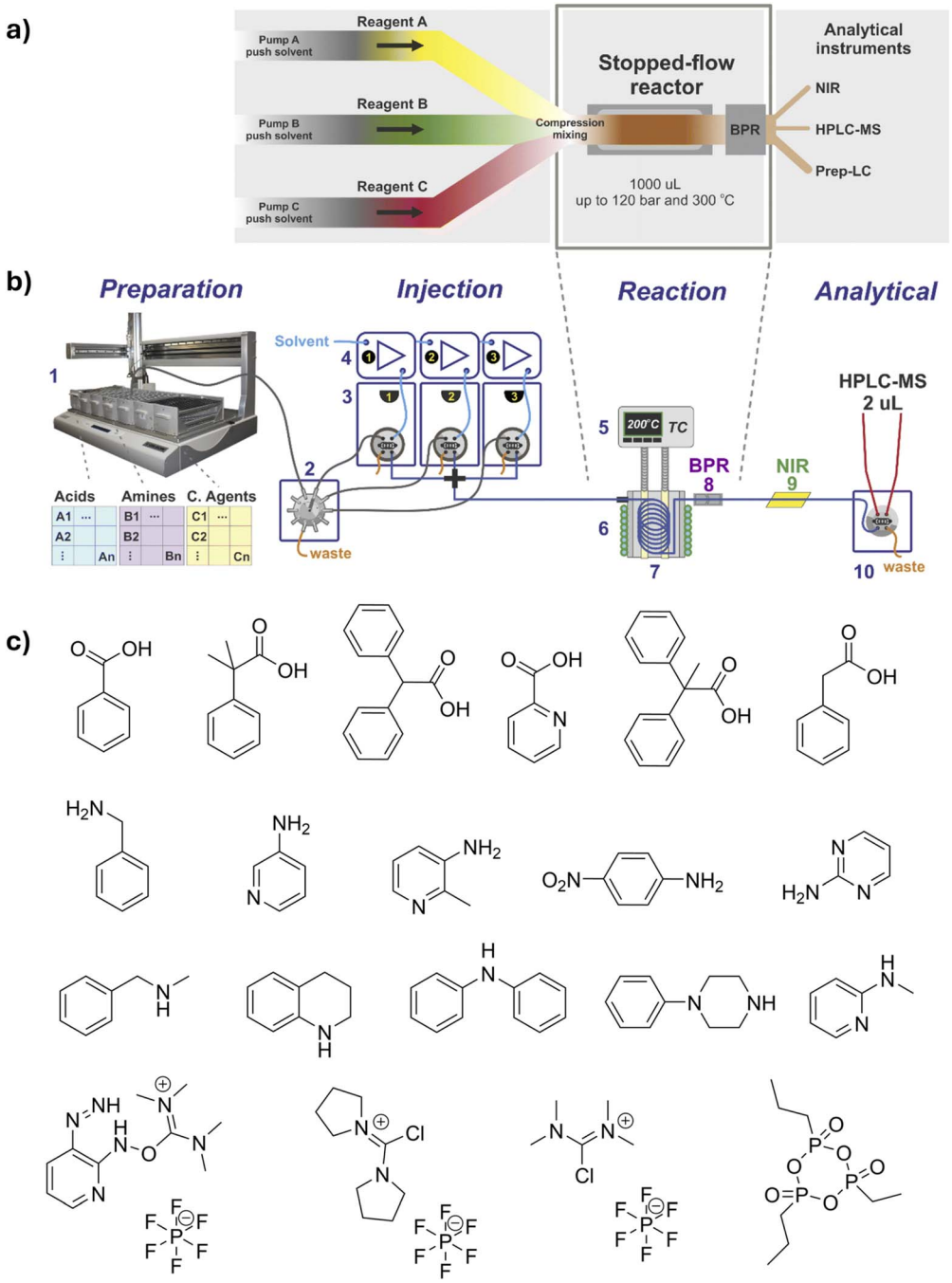

Fig. 12 High throughput platform devised by Avila *et al.*, (a) a stopped-flow system concept, (b) a high-throughput platform: a (1) liquid handler; (2) multi-selection valve; (3) array of sampling loops, each connected to a (4) respective HPLC pump; (5) digitally controlled reactor temperature; (6) digitally controlled cooling jacket; (7) stopped-flow reactor coil; (8) back pressure regulator; (9) NIR flow cell; (10) 2 μL sampling loop connected to HPLC-MS, and (c) carboxylic acids, amines and coupling agents used in the study – reproduced from Avila *et al.*[104] with permission from the Royal Society of Chemistry.

optimisation campaigns, where a wealth of diverse data from pre-existing campaigns exists.

Different methods have also been reported for comparable investigations into optimisation efficiency. Müller *et al.* reported the development of an open-source reaction simulator, enabling the comparison of various multi-objective optimisation algorithms.[102] Felton *et al.* similarly reported a framework, 'Summit', to compare seven machine learning strategies for the optimisation of two *in silico* benchmarks, based upon a nucleophilic aromatic substitution and a C–N cross-coupling.[103] Both approaches employ a simulated method for comparison, in contrast to the experimental approach outlined by Wagner *et al.*,[95] helping to minimise material consumption; both methods could be integrated into high throughput flow workflows, prior to commencing experimental work, ensuring selection of an optimal algorithm for the required optimisation task.

Avila *et al.* reported a machine learning guided platform for library synthesis (Fig. 12b).[104] The platform used a stop flow reactor which enabled reaction time to be independent of the flow rate, whilst also facilitating a ~90% reduction in the use of solvents and reagents. An initial DoE approach was used to identify suitable reaction conditions, with temperature highlighted as a key reaction parameter. A library of 25 amides was then synthesised using the platform; each of the 25 combinations of acids and amines used to synthesise these amides were subjected to four coupling reagents and nine reaction conditions, leading to a total of 900 reactions to execute, over a ~192-hour duration (Fig. 12c). The platform enabled exploration over a broader temperature range (50–200 °C) than typically achieved and/or possible when conducting the reactions in batch or alternative HTE setups. These experimental data were then used to build a machine learning model capable of predicting synthesis conditions, with 92% accuracy.

Konan *et al.* reported the use of a similar system capable of screening both discrete and continuous variables (Fig. 13B),[105] for the optimisation of a thermal sensitive [3 + 3] cycloaddition.[106–109] The optimisation strategy adopted was categorised into three distinct stages: sampling, filtering and optimisation. Initially, solvent–catalyst combinations were selected and subsequently screened *via* the use of a two-way ANOVA (analysis of variance) and DoE, with the reaction conditions then optimised using a feedback algorithm. The authors commented on the advantages of using ANOVA and

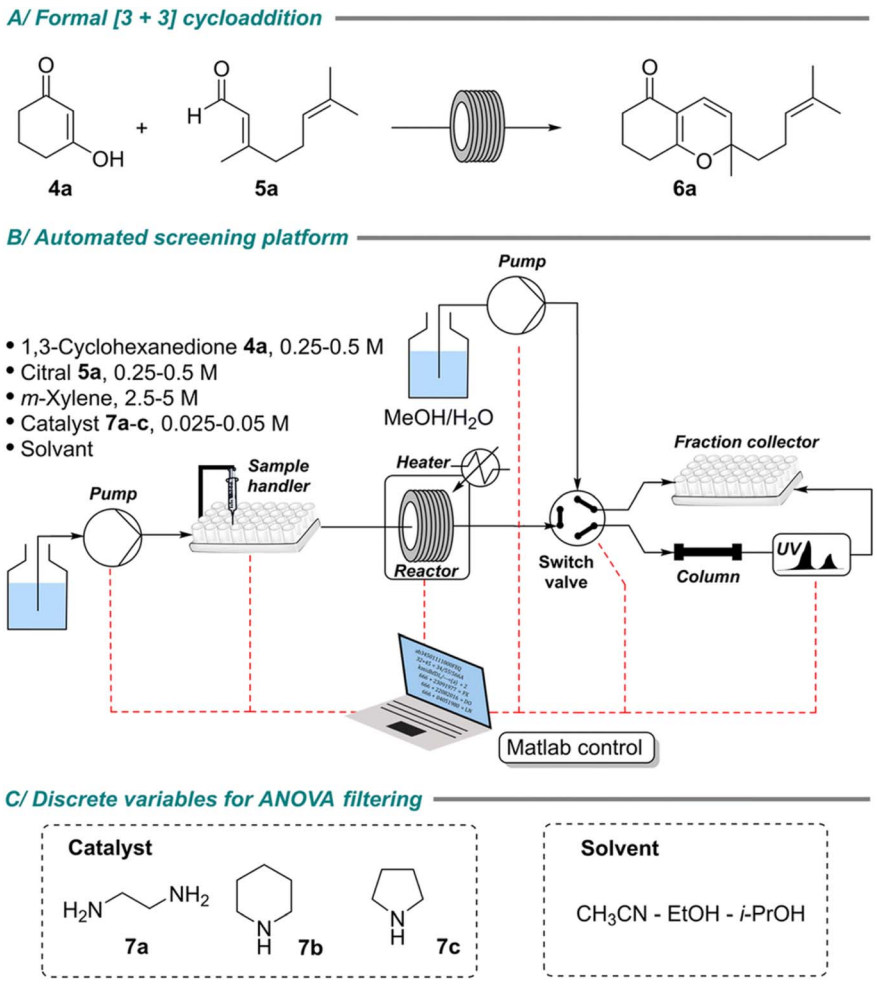

Fig. 13 (A) Benchmark [3 + 3] cycloaddition; (B) the automated screening platform used for study; (C) the list of discrete variables investigated – reproduced from Konan *et al.*[105] with permission from the Royal Society of Chemistry.

DoE based screening in HTS, in contrast to 'brute force' approaches as reported in some of the examples outlined herein, due to the ability to capture the effect of continuous variables across all discrete variables. Four continuous variables (temperature, residence time, equivalent of Fig. 13: **4a**, and catalyst loading) and two categorical variables (catalyst and solvent) were considered for the optimisation of a [3 + 3] cycloaddition benchmark reaction (Fig. 13A).

The manual selection of solvents and catalysts was implemented prior to sampling *via* LHC (Fig. 13C). Screening of the continuous variables across the nine possible combinations of solvents and catalysts was conducted over 45 experiments, in a ~29-hour window with ~1 mmol of Fig. 13: **4a** consumed (190 μL injection volume, <30 μmol of Fig. 13: **4a** per injection). A two-way ANOVA was then used to filter the results of the screening; two discrete combinations were selected for subsequent self-optimisation. An optimisation algorithm based upon a modified Nelder–Mead method was used,[110] with the reaction optimised in both ethanol and iso-propanol. The optimal experimental conditions in both solvents were found to be comparable: for ethanol, an optimal HPLC yield of 96%, throughput of 11.9 g h^{-1}, and space-time-yield of 2.4 kg h^{-1} L^{-1} were obtained within 13 experiments across ~3 hours, with ~460 μmol of Fig. 13: **4a** consumed; for isopropanol, an optimal HPLC yield of 79%, a throughput of 11.7 g h^{-1}, and a space-time-yield of 2.3 kg h^{-1} L^{-1} were achieved, within 18 experiments across ~4 hours with ~660 μmol of Fig. 13: **4a** consumed. The optimised ethanol conditions were subsequently scaled up in flow with good success, affording 7.8 g of the desired product (Fig. 13: **6a**) in 30 minutes (85% isolated yield, 15.6 g h^{-1}). The wider applicability of the optimised procedure was also demonstrated across a range of starting materials with good success – isolated yields were in the range of 79–83% and throughputs in the range of 15.9–21.6 g h^{-1}.

In collaboration with Pfizer, Eyke *et al.* outlined a platform for both reaction optimisation and kinetic evaluation, using both droplet micro-fluidics and parallel reactor channels (Fig. 14),[111] based upon a previously reported platform by the Jensen group.[91] To facilitate a high throughput, a bank of multiple independent parallel reactors was introduced, with each reactor capable of independent operation across differing conditions. A stopped flow approach was employed in a similar manner to that of Avila *et al.*[104] and Chatterjee *et al.*,[79] with software controlling the scheduling of the droplets to prevent bottlenecks in the platform.

The platform's suitability for kinetic studies was first investigated *via* the reproduction of a previously conducted kinetic investigation of a nucleophilic aromatic substitution (S_NAr) reaction.[112] Ten parallel reactors were used for the study, with the platform successfully determining the kinetic parameters, with excellent agreement with the previous study, in 30 reactions across a 13-hour window of platform time with only 600 mg of starting materials consumed.

Closed-loop automated optimisation was subsequently attempted with the open-source Bayesian optimisation package Dragonfly.[113] A Buchwald–Hartwig amination was investigated

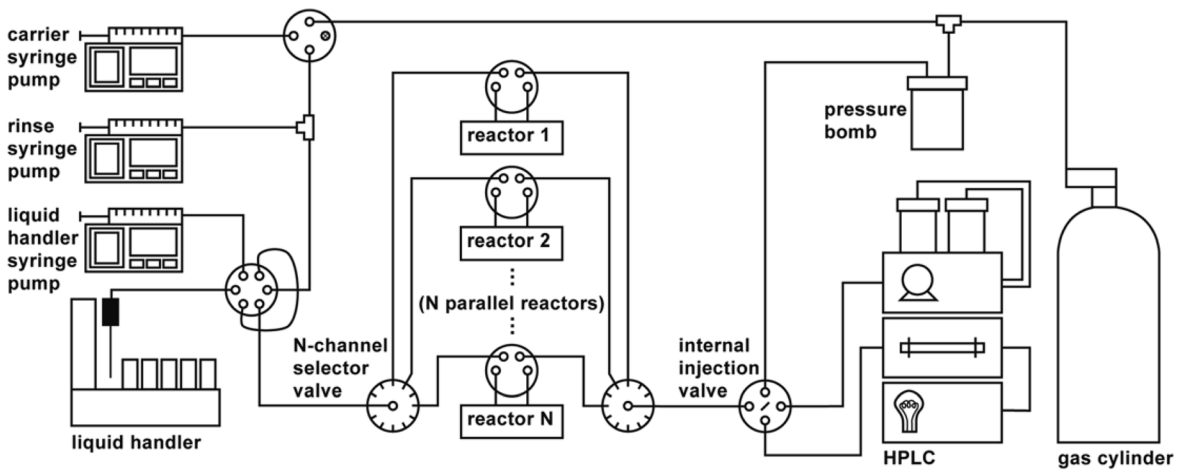

Fig. 14 Schematic representation of the outlined platform with N parallel stationary reactors – reproduced from Eyke *et al.*[111] with permission from the Royal Society of Chemistry.

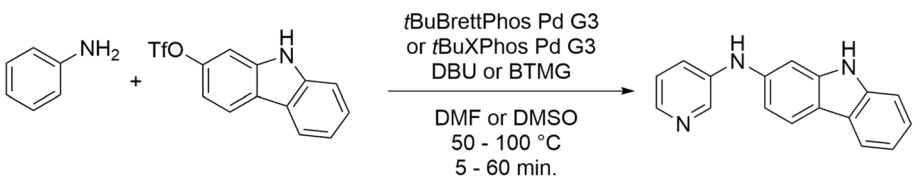

Scheme 6 Buchwald–Hartwig amination between 9*H*-carbazol-2-yl trifluoromethanesulfonate and 3-aminopyridine – adapted from Eyke *et al.*[111] with permission from the Royal Society of Chemistry.

as a test reaction, with the use of two palladium catalysts (*t*BuBrettPhos Pd G3 and *t*BuXPhos Pd G3) and two bases (DBU and 2-*tert*-butyl-1,1,3,3-tetramethylguanidine (BTMG)), explored across two solvent systems – dimethylformamide (DMF) and dimethyl sulfoxide (DMSO) – and a range of temperatures (50–100 °C) and residence times (5–60 minutes) (Scheme 6). Optimal conditions for DMF were found in 28 experiments across a 12.5-hour window, with 132 mg of starting material consumed; optimal DMSO conditions required 30 experiments across a 14-hour window with a consumption of 142 mg of material. In comparison to nanowell plates, the moderate sample throughput was noted by the authors, with comments on the potential sources of improvement: increased instrumentation, such as liquid handlers, for solution preparation, and HPLC instruments, for analysis, to prevent bottlenecks; further optimisation of the scheduling software; and shorter analytical methods and liquid handling times.

Florit *et al.* expanded upon this work in the development of a dynamic experiment optimization method (DynO) in a Bayesian optimisation framework.[114] The concept of dynamic flow experiments is centred around the adjustment of process inputs throughout a run in a controlled manner in order to collect transient data, negating the need to reach a steady state prior to data collection.[27]

To highlight the capabilities of DynO, a test reaction between a di-halogenated species and phenylboronic acid was conducted in a simulated reactor. DynO was compared with Dragonfly,[113] paired with a random optimiser, across a variety of case studies centred upon this reaction. Across these case studies DynO was run for a maximum of 10 iterations after initial data points for the Gaussian process model were collected ('initialisation'), and Dragonfly for a maximum of 65 iterations. In the majority of cases DynO learned faster than Dragonfly, in terms of both experimental time and the volume of reagent consumed, whilst in all cases initialising DynO with dynamic experiments reduced the 'relative regret' (the ratio of the difference between the achieved and optimal value, relative to the optimal value[115]) against the number of data points, experimental time, and the volume of reagents required for the optimisation.

DynO was then investigated experimentally *via* a base catalysed ester hydrolysis reaction. The design space consisted of two variables: residence time and equivalents of the base relative to the ester, between 5–30 minutes and 1–3 equiv. respectively. A steady state was established prior to initialisation. Then, the continuous variables were autonomously varied to obtain data for initialisation, which were then used to train the Gaussian process. A steady state was once again established prior to commencing optimisation. Optimal conditions were obtained after one iteration with an experimental yield of 93% obtained, with a corresponding residence time of 30 minutes and 2.4 equiv. of the base.

Whilst this review primarily focuses on high throughput experimental flow procedures, high throughput computational approaches can also be adopted.[116–121] This has been highlighted in work by Coley *et al.*,[122] and Nambiar *et al.*,[123] who used a computer-aided synthesis planner (CASP), trained on millions of reactions from the Reaxys database and the U.S. Patent and Trademark office, to provide and evaluate the potential success of suggested reaction conditions. However, the study by Coley *et al.* required additional input from the chemist,[122] regarding variables such as residence time, stoichiometries, and concentrations, to ensure compatibility with flow chemistry. The reactions were then carried out using a flexible 'plug-and-play' robotic flow chemistry platform, to accommodate a broad range of reaction classes, with the synthesis of 15 active pharmaceutical small molecules, in reasonable yields (32–95%) and throughputs (265 mg h^{-1}–1.72 g h^{-1}).

Nambiar *et al.* expanded upon this work, adopting Bayesian optimisation (Dragonfly package) for the self-optimisation of both continuous and discrete variables for the CASP suggested routes, although manual solubility screening was still required. A telescoped multi-step synthesis of the active pharmaceutical ingredient sonidegib (Fig. 15: **6**) was targeted, with the top ranked suggested route consisting of a S_NAr reaction, followed by a nitro reduction and a subsequent amide coupling (Fig. 15). A robotic modular flow chemistry system, similar to that in a previous study, was used to carry out the synthesis, with the addition of a faster robot and capabilities for in-line/online analysis and feedback optimisation. Before undertaking the optimisation campaign, a study was conducted to establish the stability of the palladium catalyst required for the reduction step; this preliminary study identified the deactivation of the catalyst due to the prior S_NAr reaction, and so the process was

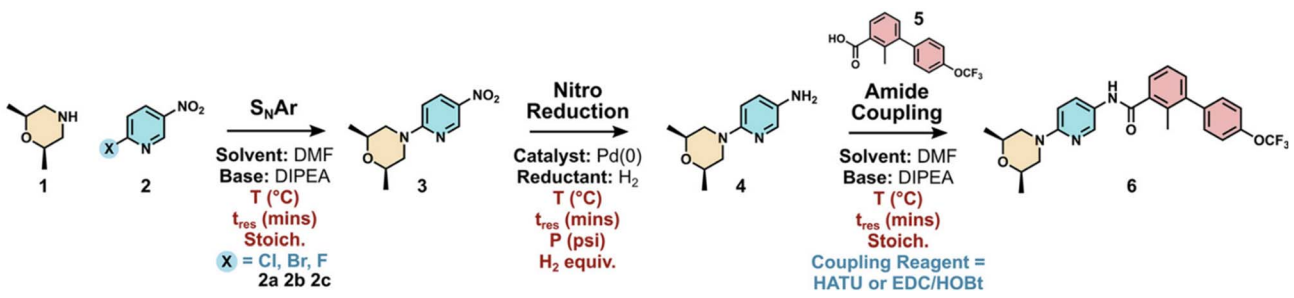

Fig. 15 CASP proposed reaction conditions, with continuous variables highlighted in red and discrete variables highlighted in blue. Abbreviations: HATU (hexafluorophosphate azabenzotriazole tetramethyl uronium), EDC (1-ethyl-3-(3-dimethylaminopropyl)carbodiimide), and HOBt (1-hydroxybenzotriazole). Reproduced from Nambiar *et al.*,[123] with permission under the Creative Commons Attribution license (CC-BY-NC-ND 4.0). Copyright © 2022 Nambiar *et al.*

divided into two, with the S_NAr reaction optimised separately to the subsequent two steps.

For the S_NAR reaction, 30 reactions were conducted over a 10-hour window, with ~0.4 g of starting materials consumed per experiment – four continuous variables (residence time, temperature, equivalents of Fig. 15: **1**, and equivalents of the base) and one discrete variable (Fig. 15: **2a**, **2b** or **2c**) were considered. Three optimisation objectives were targeted: reaction yield, productivity, and cost of reagents per mole of products made. The optimisation campaign returned two optimal objective trade-offs (**2c**, 98.3%, 5.97 g h^{-1}, \$595 per mol; **2a**, 93.8%, 5.70 g h^{-1}, \$414 per mol), with the chemist then able to select a preference based upon additional context and process considerations.

For the optimisation of the telescoped nitro reduction and amide coupling, an investigation into the formation of an unwanted side product was carried out. It was found that formation of the observed side product could be minimised *via* activation of Fig. 15: **5** in a separate reactor, prior to the coupling reaction. This led to a process configuration alteration, which was easily adopted due to the flexibility of the flow platform used. The self-optimisation campaign consisted of 15

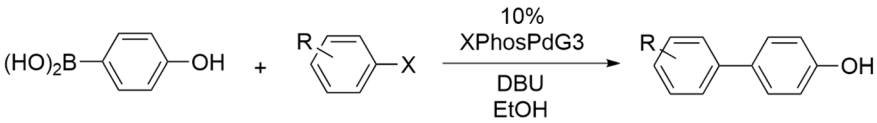

Scheme 7 Suzuki–Miyaura cross-coupling reaction investigated by Jaman *et al.*[134] Copyright © 2018 Wiley-VCH Verlag GmbH & Co. KGaA. Used with permission from Jaman *et al.*[134] High throughput experimentation and continuous flow validation of Suzuki–Miyaura cross-coupling reactions, *Chemistry – A European Journal*, Wiley-VCH Verlag GmbH & Co. KGaA.

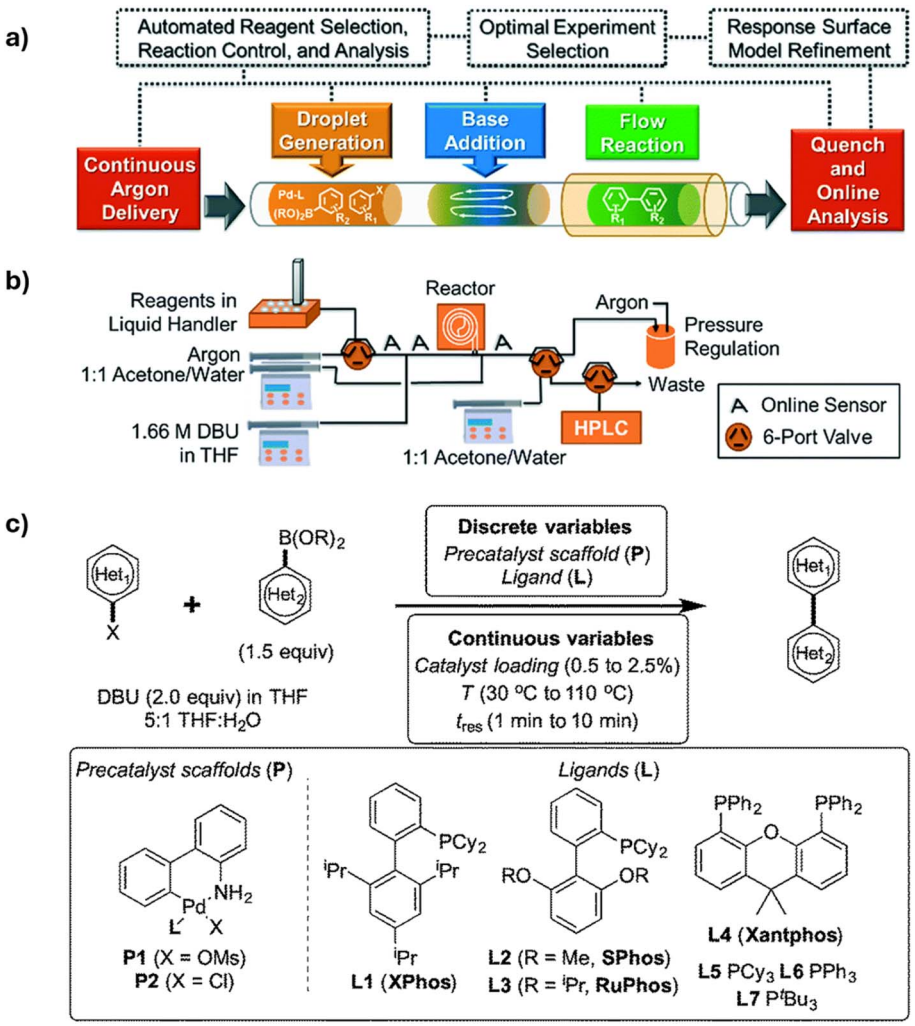

Fig. 16 (a) Concept and (b) flow diagram for automated Suzuki–Miyaura cross-coupling optimization and (c) optimisation scheme for Suzuki–Miyaura cross-couplings in the presence of DBU and THF/water – reproduced from Reizman *et al.*[135] with permission from the Royal Society of Chemistry.

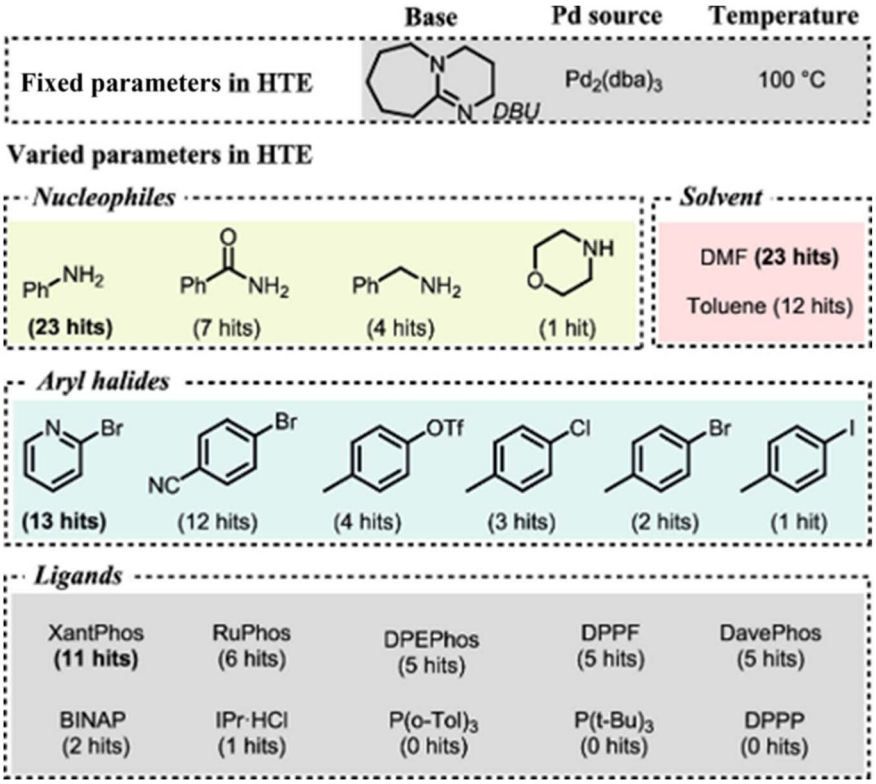

Fig. 17 HTE screening parameters, with reference to the number of hits identified for each – reproduced from Kashani *et al.*[137] reprinted with permission from Kashani *et al.*[137] Copyright © 2020, American Chemical Society.

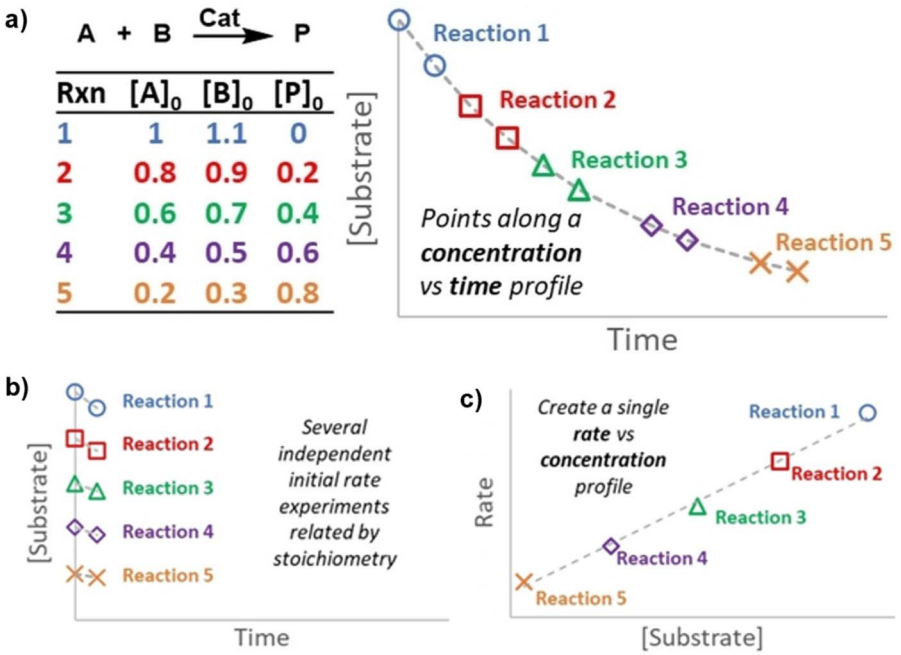

Fig. 18 Relationship between independent initial rate experiments and a single kinetic profile through SPKA. Each colour represents a new reaction, a simulated point on a single kinetic profile collecting in either batch or flow: (a) concentration *vs.* time plot for one experiment monitored over time; (b) concentration *vs.* time plot for multiple independent reactions; (c) multiple reactions creating a single SPKA kinetic profile in a rate *vs.* concentration plot. Reproduced with permission under the Creative Commons Attribution license (CC-BY). Copyright © 2023 Lennon and Dingwell,[138] *Angewandte Chemie International Edition* published by Wiley-VCH GmbH.

experiments over 13 hours, consuming ~1.4 g of starting material per experiment. Reaction yield and throughput were used as optimisation objectives, with five objective variables targeted: three continuous (residence time for the activation of Fig. 15: **5**, equivalents of Fig. 15:**3** and temperature of the amide coupling) and two discrete (reagent for the activation of Fig. 15: **5** and reactor volume for the amide coupling). An optimal yield and throughput of 93% and 7.4 g h^{-1} of sonidegib was achieved.

When algorithmic optimisation is paired with flow chemistry, such as in the outlined studies above, complex relationships between variables can be deciphered and processes optimised in a timely manner. The ability to conduct reactions under slug flow regimes also enables minimal material consumption throughout the optimisation process. This is particularly useful in reactions with multiple, complex parameters and/or expensive reagents – for example, in the case of complex catalytic reactions.

Flow HTE in catalysis

The discovery and use of new synthetic methodologies dates back over 150 years.[124] However, within recent times the prevalence of synthetic methodology studies has drastically increased.[125,126] HTE can prove particularly useful in such studies, especially in the case of a complex synthetic methodology, where a variety of factors can interact to alter the success of a reaction.[127] This is particularly true in the case of catalytic reactions, that consist of numerous steps and competing pathways,[128] making traditional OFAT optimisation challenging. Catalytic reactions, such as many cross-coupling reactions, are central to pharmaceutical, agriculture, and detergent industries,[129] and as such much work has been conducted to screen these reactions. The advantages of flow chemistry for catalysis have already been demonstrated, including increased reaction rates due to enhanced mass transfer and high local concentrations of the catalytic species,[130] reduced by-product formation due to improved process control,[131] and enhanced scale up capabilities *via* scaling up, scaling out or numbering up.[132]

In HTE, the most commonly investigated transformation is the Suzuki–Miyaura cross-coupling reaction.[48] The reaction is considered one of the most important carbon–carbon bond forming reactions, facilitating the synthesis of a large variety of organic compounds across various fields.[133] However, the reaction is highly dependent on the substrates employed,[26] meaning HTE can prove helpful in identifying the key reaction parameters, by screening several conditions simultaneously. Jaman

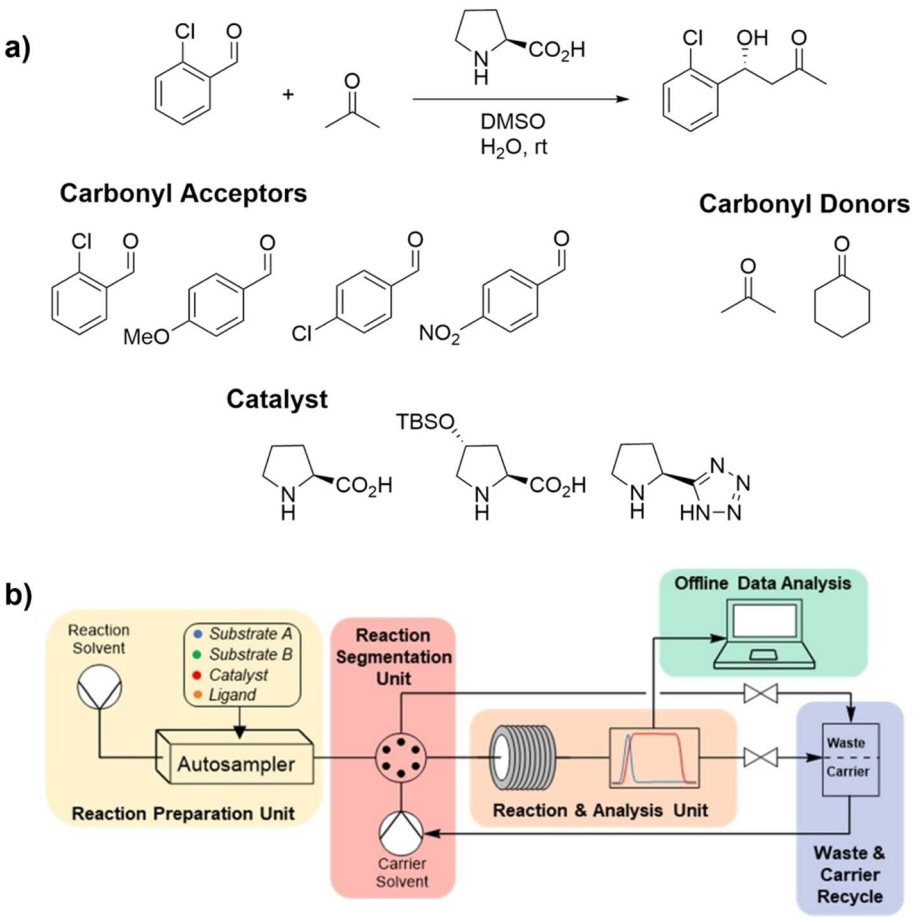

Fig. 19 (a) Proline catalysed aldol reaction and scope of kinetic and mechanistic screening and (b) schematic diagram of the flow platform employed for SPKA kinetic analysis. Reproduced with permission under the Creative Commons Attribution license (CC-BY). Copyright © 2023 Lennon and Dingwell,[138] *Angewandte Chemie International Edition* published by Wiley-VCH GmbH.

et al. highlighted the use of batch HTE with continuous flow validation for investigation of this reaction class.[134] In one hour, the automated HTE platform performed reactions in a 96-well plate, using 4-hydroxyphenylboronic acid and 11 different aryl halides for the cross-coupling, at temperatures of 100 °C, 150 °C, and 200 °C (Scheme 7). Reactions were selected from each of the hotspots from the HTE campaign to establish confidence levels between batch HTE and continuous flow.

A 1 : 1 ratio of 4-hydroxyphenylboronic acid and aryl halide was adopted across all flow reactions; residence times of 0.5, 1, 3 and 6 minutes were explored for each reaction, at either 100 °C or 150 °C. A Chemtrix chip reactor was used for this investigation, which subsequently required a decreased catalyst loading of 0.5%, in order to prevent clogging of the reactor. The findings of the microfluidic evaluation were found to be comparable to the results of the HTE screening, with negative results also validated *via* flow.

Reizman *et al.* reported an automated droplet microfluidic platform (Fig. 16a) for the optimisation of a variety of Suzuki–Miyaura reactions (Fig. 16b).[135] Samples of pre-catalysts, excess ligands, aryl halides with an internal standard, and boronic acid or boronic pinacol esters were prepared in tetrahydrofuran (THF), and stored under argon in an automated liquid handler. The liquid handler prepared droplets *via* the sampling and mixing of the corresponding stock solutions, followed by injection into a sample loop, with the droplets progressed *via* argon. To initiate the reaction, DBU was injected into the droplet and the reaction mixture heated in a Teflon tube reactor. The droplet was subsequently quenched, sampled, filtered and split, with one sample used for UV quantification and one for MS analysis.

The system was controlled and optimised *via* software that formulated response surface models in an iterative manner and proposed experiments based upon online HPLC data, within the confines of the selected discrete variables and continuous variable ranges. The optimisation aimed to maximise the turnover number (TON), a metric used to describe the maximum use of a catalyst for a specific transformation under defined reaction conditions,[136] whilst maintaining 90% of the maximum yield, within a maximum of 96 experiments. Of the four examples explored as part of this study, three returned yields over 82% with max TON values of over 69, with only the final example returning a low yield of 35% with a max TON value of 17.

The Buchwald–Hartwig amination reaction is the second most targeted transformation in HTE,[48] and is commonly used to validate system suitability, such as in the case of the previously outlined study from Eyke *et al.*[111] Kashani *et al.*

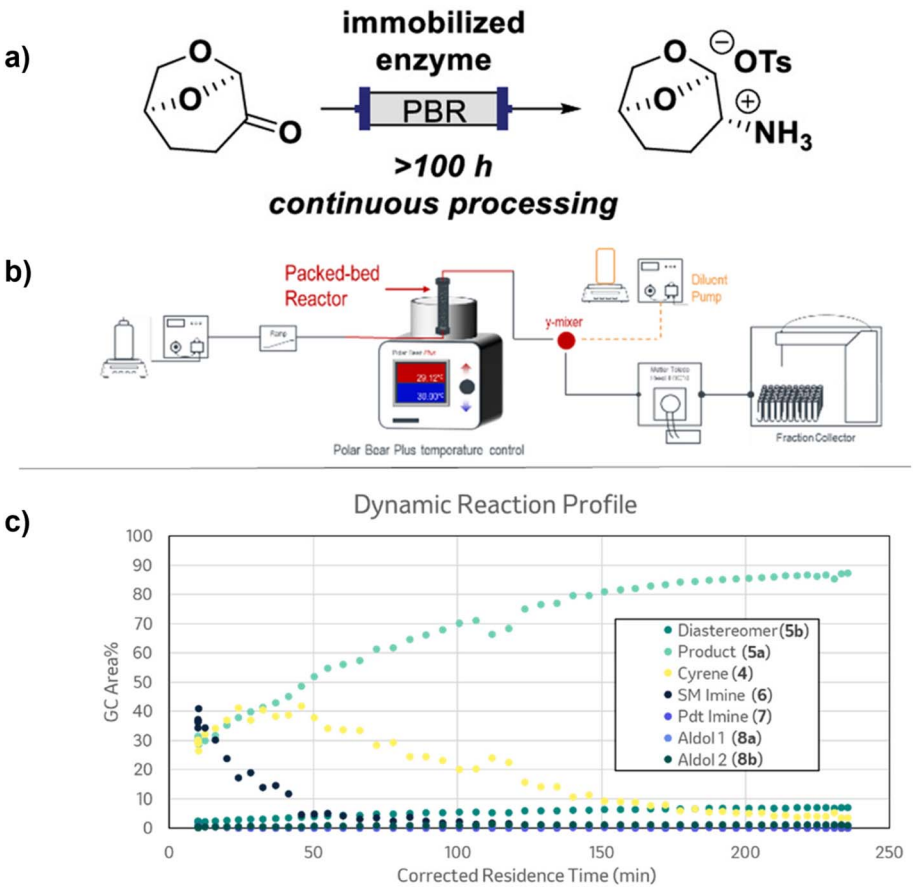

Fig. 20 (a) Reductive amination of cyrene and (b) process flow diagram of the dynamic flow platform. (c) Reaction profile as a function of the corrected residence time calculated for each fraction – adapted with permission from Di Maso *et al.*[149] Copyright © 2024 American Chemical Society.

investigated the transformation using HTS (Fig. 17), incorporating both batch and flow chemistry, to develop an improved synthetic methodology that could also be applied to a wider selection of cross coupling reactions.[137] As part of this screening, each combination of six differing organohalides, four amine nucleophiles, 10 commercially available ligands, and two solvents was explored, with certain parameters fixed to keep the number of experiments within a reasonable range. Five 96-well plate reactors were used for the screening of 480 experiments, with 35 hits quantified by gas chromatography mass spectrometry (GC-MS) analysis, and some hit experiments being quantified and successfully reoptimised in batch.

One of the key variable discoveries was the suitability of DBU, in conjunction with palladium and inexpensive ligands, to facilitate the transformation. The use of DBU also enabled a continuous flow chemistry approach to the reaction, as the clogging risk associated with many inorganic bases was eliminated. With certain modifications to the screening conditions, such as increased temperature and catalyst loading, a series of coupling products were generated in good to high yields (78–88% yield) using a simple 1 mL tubular reactor. This approach was also applied to the Mizoroki–Heck reaction *via* a change of base to triethylamine in dioxane at 90 °C, and the Sonogashira reaction *via* the use of triethylamine in THF at 90 °C and a 0.25 M concentration.

In 2024, Lennon and Dingwell outlined a method for the kinetic investigation of a catalytic process *via* the use of HTE in flow.[138] The authors coined the term Simulated Progress Kinetic Analysis (SPKA) for the approach, in which a singular kinetic profile is obtained from the instantaneous rate of multiple individual reactions across varying concentrations; this allows the construction of a rate *vs.* concentration plot (Fig. 18c). This work expands upon the pioneering reaction progress kinetic analysis approach developed by Blackmond;[139] comparative kinetics investigations have also been reported in flow, across various groups.[140–145] The SPKA approach was used to investigate the kinetics of an asymmetric organocatalysis transformation in the form of a secondary amine mediated aldol reaction (Fig. 19a).[146] The time taken to collect data is independent of reaction time, so monitoring of reactions in their entirety is not required. Lennon and Dingwell noted that "SPKA is agnostic to the experimental approach",[138] meaning SPKA can be conducted in both batch and flow.

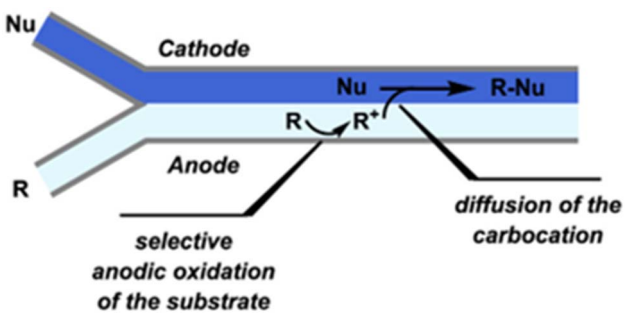

Fig. 21 Selective anodic substitution reaction due to selective wetting of the anode and cathode – reproduced from Noël *et al.*[156] with permission under the Creative Commons Attribution license (CC-BY-NC-ND). Copyright © 2019 American Chemical Society.

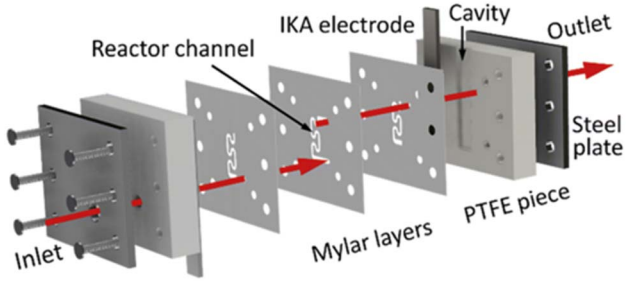

Fig. 22 Top: schematic view of the all the layers that form the microreactor – reproduced from Rial-Rodríguez *et al.*[164] with permission from the Royal Society of Chemistry.

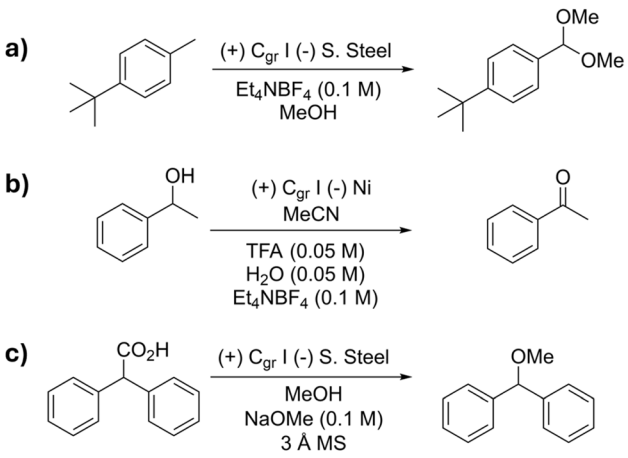

Scheme 8 Electrochemical transformations explored by Rial-Rodríguez *et al.*:[164] (a) oxidation of *tert*-butyltoluene, (b) oxidation of alcohol to corresponding ketone, (c) Hofer–Moest reaction of carboxylic acid – reproduced from Rial-Rodríguez *et al.*[164] with permission from the Royal Society of Chemistry.

The system was validated using flow chemistry, using a segmented flow regime (Fig. 19b). To collect the SPKA profile, ten reaction segments were created – a single 0% reaction segment, without any catalyst as a reference point, and nine reaction segments with decreasing reagent concentration, spaced equally for a simulated 0–80% conversion. The segments were passed through a reactor coil prior to analysis of the outlet concentration *via* in-line infrared (IR) spectroscopy. The known inputs and measured outputs were used to generate a 9-point SPKA profile, which was in good agreement with a two-point batch SPKA profile. A decrease in residence time was also investigated with the resulting data in good agreement with previously reported kinetic data for the transformation.[147,148]

The platform was further optimised by reducing the number of data points per profile to 5 whilst operating at a lower residence time and delay time between slugs, enabling the generation of a kinetic model in 25 minutes, with a total reaction volume of 0.75 mL, equating to 57 kinetic profiles per day when run for 24 hours. Lennon and Dingwell highlighted the

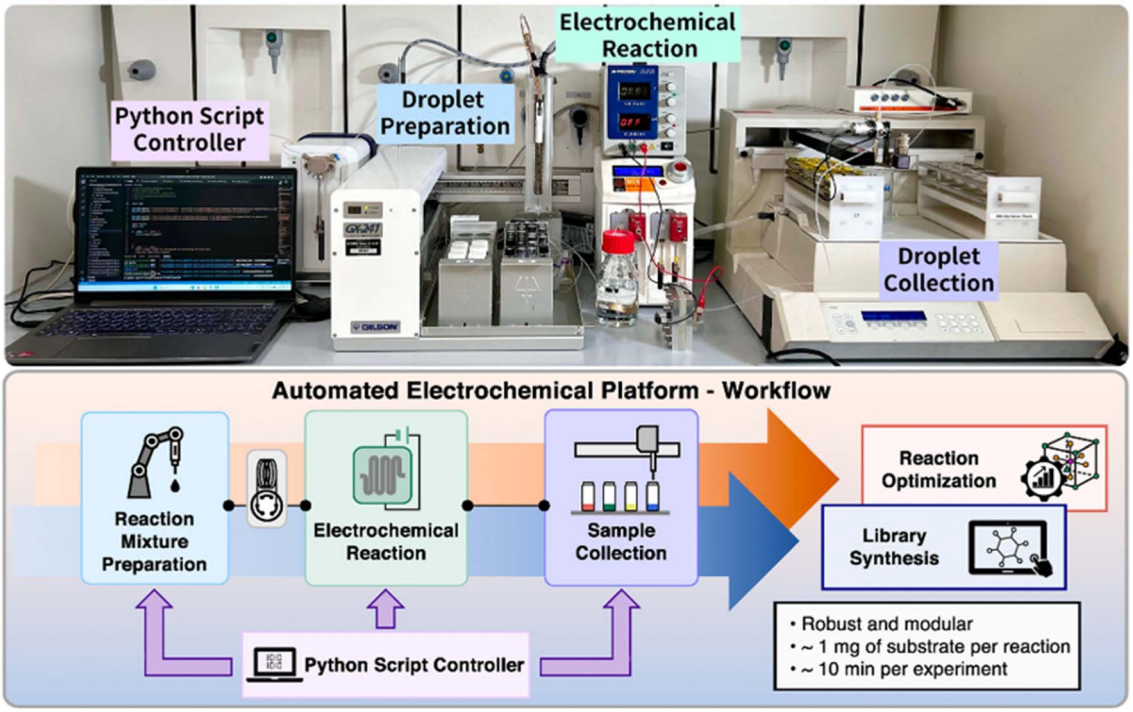

Fig. 23 Picture and schematic representation of the slug based automated electrochemical platform – reproduced with permission under the Creative Commons Attribution license (CC-BY) Copyright © 2024 Rial-Rodríguez *et al.*,[165] *Angewandte Chemie International Edition* published by Wiley-VCH GmbH.

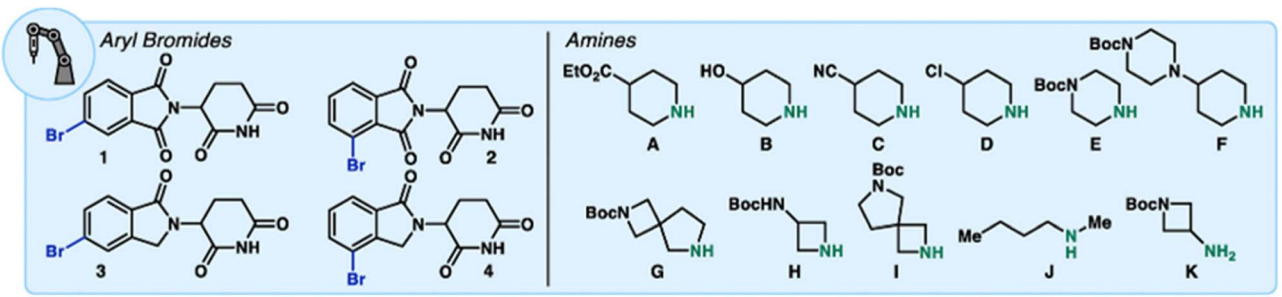

Fig. 24 Coupling partners for library synthesis – reproduced with permission under the Creative Commons Attribution license (CC-BY) Copyright © 2024 Rial-Rodríguez *et al.*,[165] *Angewandte Chemie International Edition* published by Wiley-VCH GmbH.

capabilities of the platform, conducting a kinetic investigation of the same aldol reaction (Fig. 19a).[138] The subsequent investigation consisted of 24 possible combinations, requiring three experiments per combination to determine the rate, resulting in a total of 216 experiments. The 216 experiments were conducted in 90 hours, in comparison to the ~3500 hours the same experiments would have taken if conducted in a traditional manner. The investigation provided valuable information regarding catalyst deactivation and unwanted off-cycle processes.

Scientists from Merck used a similar approach for the translation of an immobilised transaminase process (Fig. 20a) from batch to flow,[149] due to inefficiencies in the batch procedure. Di Maso *et al.* used a packed-bed flow reactor to facilitate the transformation, employing a dynamic flow method to optimise the reaction. DoE was used to optimise and obtain further reaction understanding in batch prior to translation to flow. A residence time of 4 hours was required to reach full conversion, meaning a pseudo steady state was reached after 22.5 hours, rendering optimisation under the steady state unfeasible. In the dynamic flow kinetic investigation, a steady state was first reached, followed by a decrease of flow rate at a set rate until a final steady state was reached, with corresponding fractions collected and analysed by GC throughout the run (Fig. 20c). The corrected residence time of each fraction collected was calculated, with times from 30 minutes to 4 hours scanned across a ~16-hour period. A total of sixty individual conditions were investigated in the same time that 4 conditions would have taken using a traditional method.

The dynamic experiment suggested that a residence time of approximately 3 hours would return full conversion to the desired product; informed with this result, further optimisation

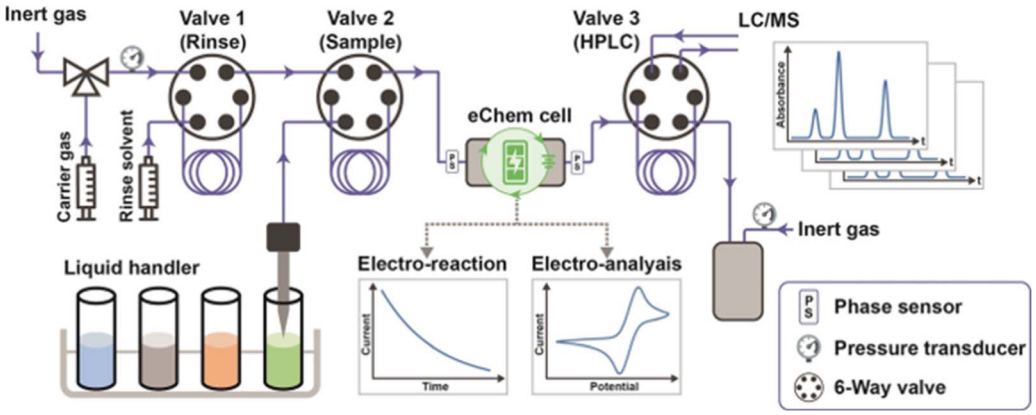

Fig. 25 Automated microfluidic platform for electrochemical reactions and analysis. Copyright © 2020 Wiley VCH GmbH. Used with permission from Mo *et al.*[162] A multifunctional microfluidic platform for high-throughput experimentation of electroorganic chemistry, *Angewandte Chemie International Edition*, Wiley VCH GmbH.

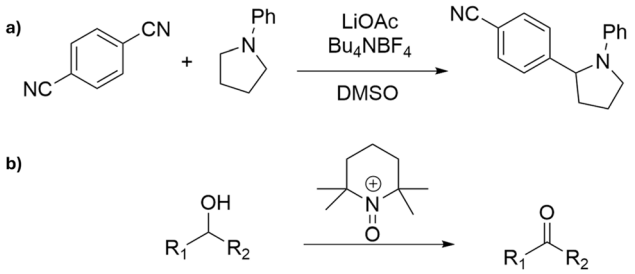

Scheme 9 (a) Electrochemical redox-neutral α-amino arylation of 1-phenylpyrrolidine and (b) the TEMPO-catalysed alcohol oxidation reaction. Used with permission from Mo *et al.*[162] A multifunctional microfluidic platform for high-throughput experimentation of electroorganic chemistry, *Angewandte Chemie International Edition*, Wiley VCH GmbH.

and process improvements were then completed. An investigation of the immobilised enzyme stability, enzyme evolution, and solvent selection was subsequently carried out, resulting in a further optimised procedure. It was identified that use of an evolved enzyme would reduce the residence time from 3 hours to 90 minutes, which could then be halved again to 45 minutes with the use of an alternative resin as a solid support for the immobilised enzyme. The isolation of the desired product was also altered, improving both the isolated yield and the diastereomeric ratio of the isolated material. The optimisation culminated in the development of a process with a 4-fold improvement to the throughput and diastereoselectivity, with improved isolation, that could be undertaken on a kilogram scale.

As demonstrated above, HTE has proven particularly useful in the optimisation of catalytic reactions that are mechanistically complex, and as such HTE has become increasingly relied upon in the field of a similarly mechanistically complex field: electrochemistry. The complexity of electrochemistry stems from formation of various primary intermediates *via* electron transfer, with subsequent cascade reactions leading to a variety of competitive products[150] added complexity arises from the solvent influence on ionic conductivity and the impact of mass transfer on reaction success.[151,152] Pairing HTE platforms with recently developed electrochemical flow cells – which are now becoming commercially available – has expanded the use of electrochemistry in reaction discovery and optimisation.

Organic electrochemistry flow HTE

The field of electrochemistry has recently seen a resurgence due to the commercialisation of standardised electrochemical equipment.[153] The field is centred around the use of electricity as a source of electrons to form new bonds,[154] enabling the activation of small molecules in a sustainable and cost-effective manner, whilst negating the need for toxic and expensive redox reagents.[155] The combination of flow with electrochemistry has facilitated improved control over reaction conditions and parameters such as mass-transfer, ohmic drop and selectivity,[155] aiding with reproducibility.[156] The improved control typically stems from passing the reaction mixture through the reactor, where mass transfer is primarily dominated by diffusion (Fig. 21). The rate of diffusion is increased within micro-reactors due to small interelectrode gaps, reducing the time taken for a given species in solution to diffuse to the intended electrode.[156] Despite these benefits, flow electrochemistry still has a way to go before generic processes are commonplace,[155] but it is hoped that HTE can help increase the prevalence of such processes.[153]

Automated platforms within electrochemistry are comparatively underdeveloped, with only a limited number of high throughput platforms reported,[157–162] and even fewer providing a fully practical solution for HTE applications.[163] One of the main contributors to the current state of the art within the field is the Kappe group who, in collaboration with Merck, have reported two separate screening platforms.[164,165] The initial platforms consisted of a low-volume electrochemical microreactor (Fig. 22), with an internal volume of 17 μL and interelectrode gap of 0.3 mm, operated at a residence time of 7.3 seconds. The reactor consumed minimal reaction material, with only 0.7 mg consumed per reaction, and could conduct 40 experiments in approximately 2 hours.

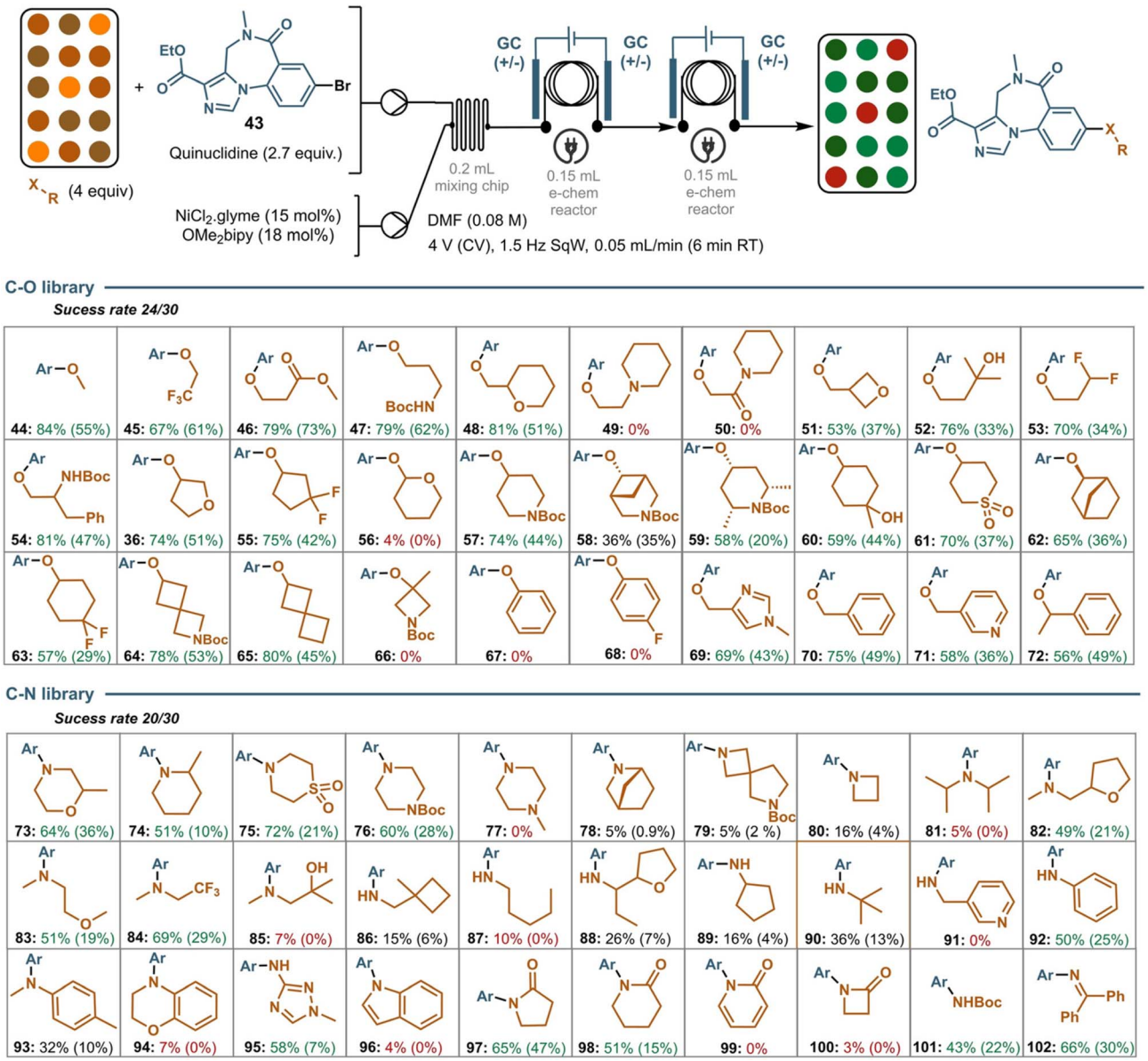

Fig. 26 Automated library application of the outlined platform – CO and CN functionalization of bromo-flumazenil (LCMS integration reported (high-throughput purification yields in brackets)) – copyright © 2024 Wiley Used with permission from Morvan *et al.*,[170] Electrochemical C–O and C–N arylation using alternating polarity in flow for compound libraries, *Angewandte Chemie International Edition* published by Wiley-VCH GmbH.

The reactor was combined with a syringe pump, power supply and fraction collector, with all devices controlled using a Python script from a singular computer. Reactions were analysed *via* HPLC analysis, with a fraction collector used to facilitate efficient at-line analysis. The ability to generate large datasets within short time frames enabled the incorporation of statistical analysis software. Multiple linear regression models were employed for yield, productivity, and current efficiency outputs, predicting results within the design space, with visualisation capabilities in the form of surface plots.

Three electrochemical reactions were chosen as case studies to model the suitability of the system (Scheme 8); for each, 42 reactions were carried out in a fully autonomous manner. Reagent consumption per screening experiment was low across all three case studies – from 0.7–6.4 mg per experiment – facilitating efficient process design for all three reaction classes investigated. Scale up was also demonstrated *via* a Hofer–Moest reaction (Scheme 8c).[166,167] The larger electrochemical flow cell featured the same interelectrode gap as the screening reactor, but with an electrode surface area approximately 11.5 times larger. It was found that comparable yields could be achieved between the two cell sizes (83 and 85%) when the flow rate and charge were adjusted accordingly, highlighting the scalability of the method.

The Kappe group then followed up this work with the development of a droplet microfluidic platform for high

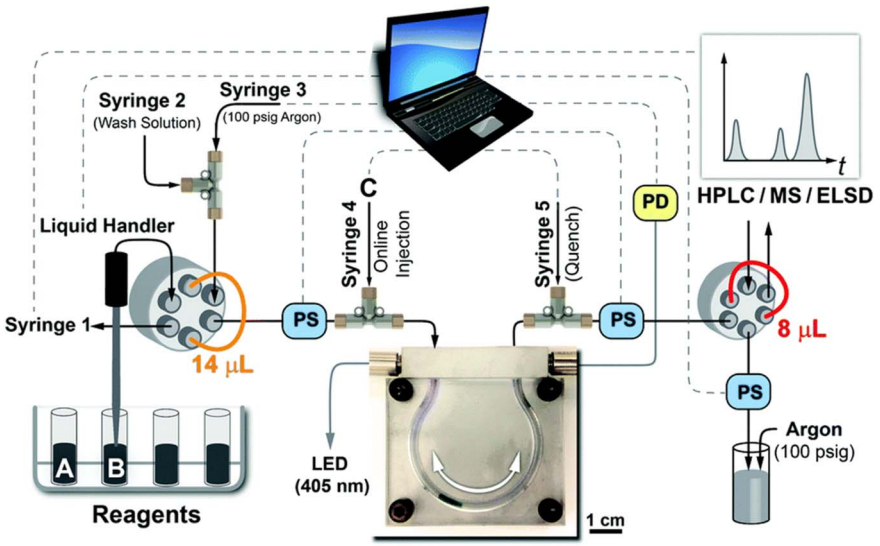

Fig. 27 Schematic diagram of the developed automated droplet-based medicinal chemistry platform, where PS indicates a phase sensor and PD indicates a photodetector. Dashed lines highlight the PC communication, grey lines highlight the optical fibres for the LED and the photodetector, and the black lines correspond to the fluoropolymer tubing for the delivery and routing of liquid droplets – reproduced from Hwang *et al.*[90] with permission from the Royal Society of Chemistry.

throughput electrochemical synthesis, using four separate modules (Fig. 23): the preparation zone, the electrochemical reaction zone, the collection zone and the script controller.[165] The reactor consisted of a simple parallel plate reactor with a 100 μm interelectrode gap and a reactor volume of 64 μL. With this system an experimental data point could be collected every 10 minutes, with a reaction time of 4 minutes, and only 1 mg of reagent consumed.

To highlight the capabilities of the platform, a Ni-catalysed C–N cross-coupling reaction was adapted from previously reported work by the Baran group.[168,169] 44 compounds were targeted, using 4 aryl bromides and 11 amines (Fig. 24), and were synthesised continuously by the automated platform in an 8-hour window. Across the 44 reactions, high amounts (>50%) of the product were detected in 15, good amounts (30–50%) in 11, and moderate amounts (10–30%) in a further 11, and only seven entries showed low or no amounts (<10%) of the desired product. These results were corroborated when transferred to a continuous flow methodology at a 0.15–0.3 mmol scale, returning 10–60 mg of the isolated product, highlighting the applicability and transferability of the platform.

Mo *et al.* also reported the development of a microfluidic HTE electrochemical platform, using computer-controlled liquid handlers to prepare microfluidic droplets of the desired reagent composition from designated vials (Fig. 25).[162] These droplets were then injected into a 15 μL sample loop, before pressurised nitrogen gas moved the droplets to the flow cell for either electrochemical reaction or analysis. The resulting droplets were then analysed *via* HPLC to determine the reaction outcome.

An α-amino C–H arylation reaction (Scheme 9a) was selected to highlight the suitability of the platform, with detailed information generated on the relationship between the reaction time and potential on product yield, obtained in as little as 10 hours with only 300 μL of reagent consumed. Subsequently, a microliter-scale cyclic voltammetry module was also developed and incorporated into the platform to probe reaction kinetics, allowing further reaction understanding *via* mechanistic elucidation. The utility of this module was then further highlighted *via* TEMPO-catalysed alcohol oxidations (Scheme 9b) in which the rapid measurement of kinetic constants of various alcohols was enabled, providing richer reaction understanding.

An electrochemical flow platform that enabled C–O and C–N arylation for compound library synthesis was reported by Morvan *et al.* (Fig. 26).[170] Reactions were conducted using a Vapourtec ion electrochemical reactor connected to an R series Vapourtec system. Following preliminary investigations into this synthesis, it was noted that the application of alternating current (AC) proved fruitful in minimising electrode fouling whilst simultaneously accelerating the reaction, with good yields and reproducibility observed when AC was employed.

Optimisation of the reaction was conducted *via* high-throughput screening in flow, with an autosampler used to automate both injections and collections. A DoE investigation was used to identify the important non-linear interactions between the chemical and electrochemical parameters, establishing the optimal reaction conditions: 2.9 eq. of base, 5 eq. of alcohol, a concentration of 0.08 M, a flowrate of 0.05 mL min^{-1}, a frequency of 0.5 Hz, 4 V, and a reaction temperature of 20 °C, which returned a conversion of 96%, a selectivity of 77%, and a 74% LC yield. These optimised conditions were then applied to the synthesis of two compound libraries, consisting of 100 diverse C–O and C–N arylation products. Reactions were conducted on 150 μmol of the material with a total reaction time per run of approximately 45 minutes; scale up was also

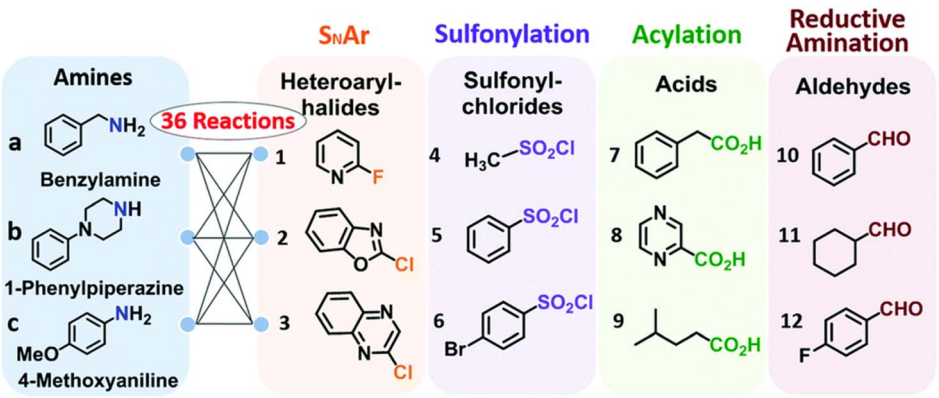

Scheme 10 Starting materials used to generate the compound library – reproduced from Hwang *et al.*[90] with permission from the Royal Society of Chemistry.

addressed, with the synthesis of one of the desired products achieved on a 10 mmol scale (2.06 g) within a 24-hour duration.

The case studies outlined herein highlight the utility of HTE in flow for fields that are still in their infancy, such as flow electrochemistry, where preexisting literature and established methods are scarce. In direct contrast, within medicinal chemistry, HTE methods are widely reported and employed, particularly within the pharmaceutical industry; many pharmaceutical companies now have specialised teams and platforms dedicated to HTE, with an increasing number adopting flow chemistry as part of these workflows.

Flow HTE in medicinal chemistry

Medicinal chemistry is centred around the design and synthesis of pharmaceutical agents that have an effect on either the human body or another living system.[171] The process of generating these agents is often highly time-consuming, expensive and challenging,[172] and as such medicinal chemists are consistently looking for new technology to simplify this approach. Over the past few decades, various new technologies have been introduced that have revolutionised approaches to laboratory-based medicinal chemistry.[173] One area that has seen rapid evolution is the method in which compounds are screened against potential therapeutic targets. With mounting pressure to deliver compounds at faster rates, there was a need to reduce the time taken to optimise lead compounds,[174] leading to HTE coupled with enabling technologies such as flow chemistry.[48] Many of the examples outlined thus far as part of this review have broader medicinal chemistry applications, due to a distinct overlap between the chemistry most applicable to HTE and medicinal chemistry. The examples outlined herein present the most apparent and direct applications of HTE and flow for medicinal chemistry purposes.

An industry study by Perera *et al.* at Pfizer reported an automated nanomole scale screening and microscale synthesis platform using flow chemistry.[175] Due to the moisture sensitivity of the chemistry, the platform was constructed in a glove box, and the study used concentrated stock solutions for each reaction component – this negated the need for multiple solutions for each solvent investigated,[176] which can be unfeasible in medicinal chemistry screening as material quantity is typically a limiting factor.[96] The stock solutions were injected in

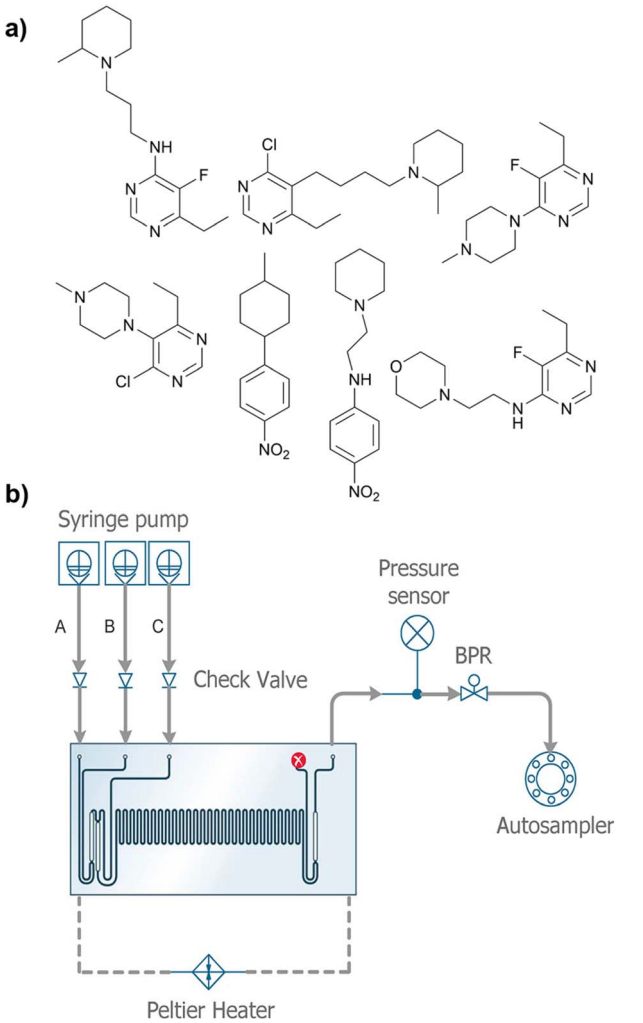

Fig. 28 (a) A selection of compounds successfully synthesised *via* flow following HTE evaluation and (b) schematic diagram of the Chemtrix BV glass chip reactor employed – reprinted from Jaman *et al.*[187] Copyright © 2020 American Chemical Society.

segments into carrier solvents, at suitable intervals to prevent cross contamination from the separate segments,[177] to evaluate the reaction solvent;[178] the diluted segments were then passed through the reactor with precise control of the flow rate, residence time, temperature, and pressure. In direct contrast to the approach broadly adopted in comparable systems, where diffusion is prevented by slug-flow regimes, each component was injected in series and allowed to diffuse together.[75] Analysis was conducted by UHPLC-MS once the segment had passed through the reactor, *via* fractionation; the method also enabled the generation of suitable quantities of material for biological evaluation.

A Suzuki–Miyaura cross-coupling reaction between 6-bromoquinoline and indazoleboronic acid was selected to validate the system, due to its prevalence within medicinal chemistry. Using methanol as the reaction solvent, the segments were heated to 100 °C, with a residence time of one minute; segments of reaction mixtures of increasing volume were generated, ranging from 5–80 μL. The segments were analysed *via* off-line LC-MS analysis with the use of four corresponding internal standards; the ratio of each of the reference standards was approximately equivalent throughout the segment, indicating that homogeneous diffusion of the reaction components into the carrier solvent had occurred across all the scales investigated.

Reaction screening was then conducted, coupling a range of electrophiles with various nucleophiles suitable for the Suzuki–Miyaura cross coupling, selected using previous knowledge from a collection of sources.[179–182] Screening of the reaction resulted in a matrix of 11 ligands (plus one blank), seven bases (plus one blank), and four solvents. The fully automated screening provided data for 5760 reactions, using 1 μL of each component stock solution per data point, facilitating 1500 reactions across a 24-hour period. From the results, data analysis was then conducted to establish trends in the reactions; successful reactions were identified, with reactions having a conversion of ≥85% deemed a successful reaction. 181 reaction conditions met this criterion for one electrophile, 103 for two electrophiles, 33 for three electrophiles, and only three sets of reactions conditions were successful across all four electrophiles. A representative reaction from the screening results was then scaled up to milligram quantities, *via* the injection of 100 consecutive segments, returning a yield of 59% (65 mg) after purification. The conditions were then further scaled up using a Vapourtec Ltd R-Series reactor, with a final yield of 42% achieved, using a simple un-optimised two pump system, highlighting the scalability of the system.

Medicinal chemists in academia have also explored the use of HTE in flow, with Hwang *et al.* reporting an automated segmented flow screening platform with the capability of rapidly generating data for a series of small, focused libraries of lead compounds (Fig. 27).[90] The platform used an oscillating flow reactor, decoupling the flow rate and the residence time, enabling multi-step and multi-phase reactions. Each reaction was run in singular microlitre scale droplets, with the technology enabling precise temperature and residence time control, showing high reproducibility, low carry over, and theoretically unlimited residence time with comparable mixing and mass transfer characteristics. Offline biological testing was employed to prevent limiting adaptability to differing assay formats. To highlight the capabilities of the platform, a variety of N–X forming reactions were performed, due to their prevalence and importance within medicinal chemistry.[183–185] Hwang *et al.* also performed a multi-phase Suzuki–Miyaura cross

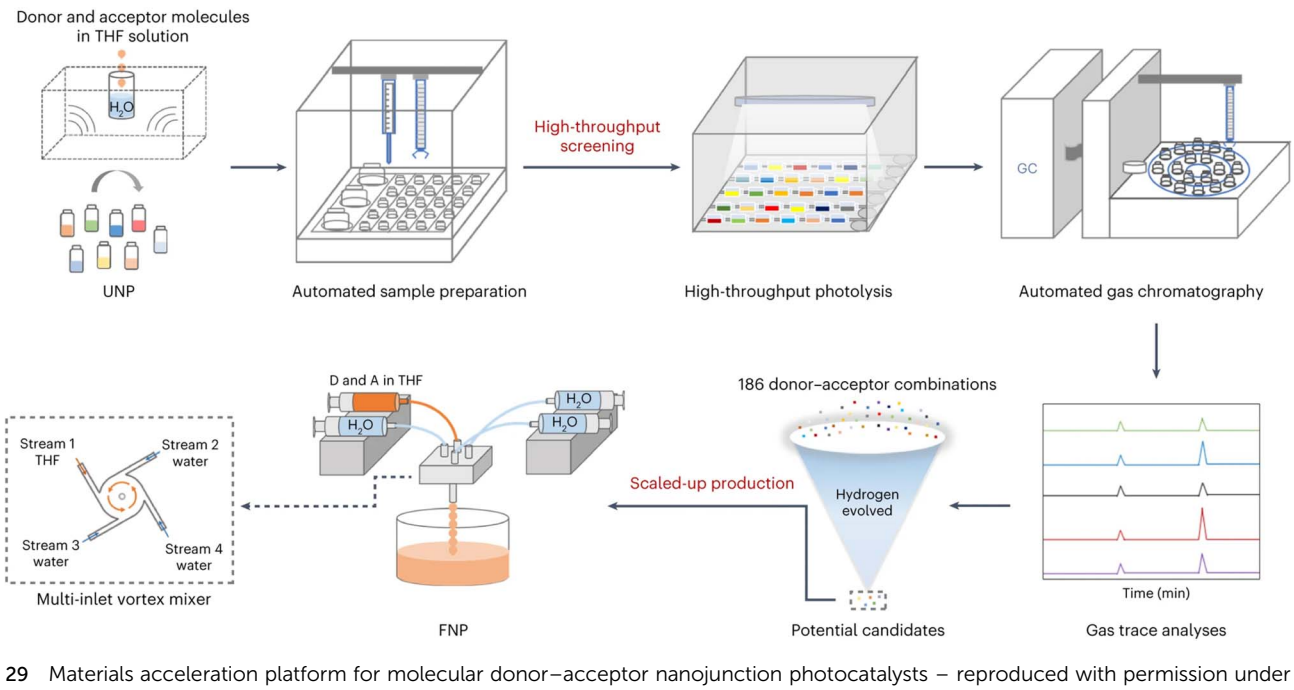

Fig. 29 Materials acceleration platform for molecular donor–acceptor nanojunction photocatalysts – reproduced with permission under the Creative Commons Attribution license (CC-BY) Copyright © 2024 Zhang *et al.*[216]

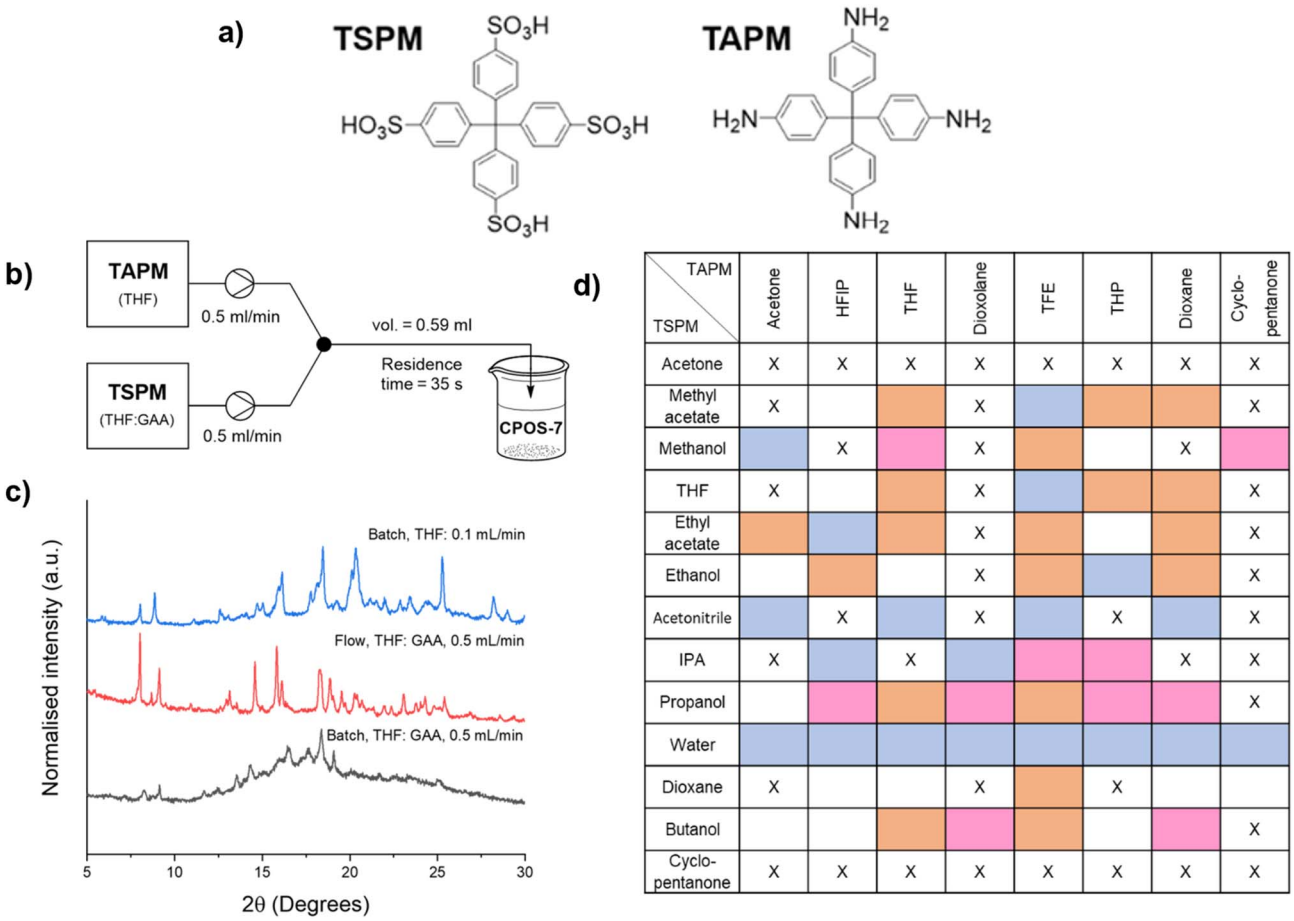

Fig. 30 (a) Structure of the salt conformers used in the study, (b) schematic diagram of the flow system employed, (c) power X-ray diffraction spectral comparison of CPOS-7 scaled under similar conditions in batch (black line) and flow (red line), and the powder X-ray diffraction for CPOS-7 in batch on decreasing the rate of addition, and (d) crystallisation conditions used during the HTS with the three main phases highlighted: orange = CPOS-7, blue = Hydrate2920, pink = unidentified phase, X = amorphous or oil, and empty = singular or unique patterns – reproduced with permission under the Creative Commons Attribution license (CC-BY) Copyright © 2023, O'Shaughnessy *et al.*,[218] *Chemistry – A European Journal* published by Wiley VCH GmbH.

coupling reaction and a multi-step synthesis of diclofenac to further highlight the scope of the platform.

The N–X forming reactions investigated were categorised into four reaction classes: S_NAr, sulfonylation, acylation, and reductive amination (Scheme 10). 36 reactions were carried out, leading to the formation of a small combinatorial compound library, varying the residence time from 1 to 20 minutes and the temperature from room temperature to 150 °C. Good conversions, with high reproducibility, were achieved across the four reaction classes; the reactions were screened, isolated, and quantified at the approximately 100 μg scale, demonstrating the platform suitability for lead optimisation within medicinal chemistry.

A workflow for screening S_NAr reactions, another prevalent reaction class within medicinal chemistry,[186] was developed by Jaman *et al.*, focussing on the large scale capabilities of the

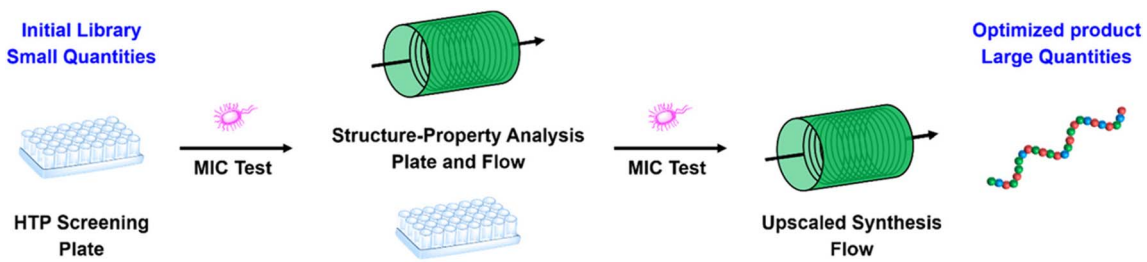

Fig. 31 Methodology for the HTE screening and upscaled production of the antimicrobial polymers – reprinted with permission from Judzewitsch *et al.*[219] Copyright © 2020 American Chemical Society.

platform.[187] The workflow was centred around the use of desorption electrospray ionisation (DESI) mass spectrometry, enabling a more rapid analysis of reaction mixtures compared to alternative analytical techniques. Two HTE methods were explored as part of the study – droplet/thin film and bulk microtiter formats – with analysis of both conducted using DESI-MS.

In the study, eight amines and 12 aryl halides were selected, with four different base conditions: *N*,*N*-diisopropylethylamine (DIPEA), sodium *tert*-butoxide, triethylamine, and no base (control). For the bulk microtiter format, 40 μL aliquots of each reaction mixture were transferred to a 384-well plate; for the droplet/thin film approach, 50 nL of each reaction mixture was transferred onto a polytetrafluoroethylene (PTFE) surface using a 384-format stainless steel pin tool. The bulk reactions were then conducted at 150 °C and transferred to the PTFE surface for analysis upon completion. The droplet reactor identified 153 successful reactions, with the bulk microtiter method identifying 311, from a total of 1536 data points; the disparity between the two methods was attributed to the heating component of the bulk method better satisfying the thermal requirement for typical S_NAr reactions.

A Chemtrix BV chip reactor (Fig. 28b) was used for further investigation of the positive results. Reactions were run at temperatures of 100 and 150 °C, with residence times between 0.5 and 5 minutes, using *N*-methyl-2-pyrrolidone as the solvent and DIPEA as the base. Formation of the desired product in flow was confirmed by both TLC and ESI-MS. The results from both the bulk and droplet screening methods were comparable to those obtained *via* the microfluidic reactions, and all 3072 reactions were completed in a 3-hour window, highlighting the viability of the workflow to screen a huge number of reaction conditions simultaneously. This approach also presents the opportunity for expanded scope, as up to 16 plates can be pinned onto one PTFE surface,[188] potentially facilitating 6144 reactions to be conducted. The utility and applicability of the workflow were further demonstrated by the groups of Thompson and Cooks, who used this technology and approach in the screening of aldol[189] and reductive amination[190] reactions, in addition to using it as a tool to facilitate the synthesis of larger compounds.[191,192]

The repetitive nature of medicinal chemistry and the typical chemistry explored during pharmaceutical pipelines lends itself particularly well to HTE in combination with flow, which is reflected in the prevalence of the technique within the field. However, the suitability of a field to HTE is not always as immediately apparent as it is in medicinal chemistry, leading to late-stage adoption of such techniques. This is particularly true within materials and supramolecular chemistry where such techniques have only recently been adopted.

Flow HTE in materials and supramolecular chemistry

Flow chemistry has found use across the full spectrum of materials and supramolecular chemistry, with non-exhaustive applications in the synthesis of quantum dots,[193,194] nanoparticles,[195,196] metal organic frameworks (MOFs),[197,198] polymers,[199,200] macrocycles,[201,202] porphyrins,[203] molecular knots[204] and cages.[205] One of the great challenges of materials chemistry is expediting the process of generating functional materials with desired properties,[206] as these properties are often only present in unique chemistries and structures.[207] Like reaction discovery, discovery of novel materials is often based on scientific intuition and expensive trial-and-error approaches,[208] leading to suboptimal discovery procedures. To combat this, the use of enabling technologies[209] and high-throughput materials experiments have become more common, enabling the efficient and cost-effective discovery-to-development of advanced materials;[210] here, the combination of HTE with continuous flow proves advantageous due to the ability to precisely control the reaction environment, resulting in minimal variability between experiments.[211]

Several groups have developed HTS platforms for the efficient discovery of new functional materials,[206,212–215] but there are fewer examples of the incorporation of flow into HTE workflows – perhaps due to the lower uptake of flow technology in general across materials chemistry. However, examples are emerging: Zhang *et al.* outlined a platform for the screening and synthesis of molecular nanojunction photocatalysts,[216] centred around the automated screening of a combinatorial molecular library, with subsequent scale up *via* continuous mixing (Fig. 29). The library contained 186 products, synthesised by the combination of molecular donors and acceptors using ultrasonic nanoprecipitation processing. These molecules were tested using a high throughput photocatalysis screening workflow, for sacrificial hydrogen evolution, over a three-day period. Here, unlike many of the examples outlined in the review, the photocatalytic properties of the synthesised samples were analysed as opposed to the success of the synthesis itself. The most active of these molecules were then scaled up using a flow-based flash nanoprecipitation (FNP) process,[217] which uses a multi-inlet vortex mixer to rapidly mix THF and water to generate nanoparticulate materials on a large scale. The activities of these materials observed in the screening experiments were mirrored in the scale up, validating the suitability of the system.

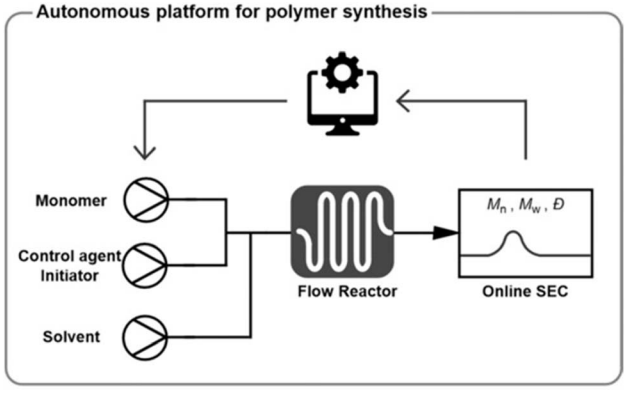

Fig. 32 Schematic outline of the developed platform for polymer synthesis – Copyright © 2019 Wiley. Used with permission from Rubens *et al.*,[220] Precise polymer synthesis by autonomous self-optimizing flow reactors, *Angewandte Chemie International Edition*, Wiley VCH Verlag GmbH & co. KGaA, Weinheim.

High throughput screening has also been reported by O'Shaughnessy *et al.* in a study of the solvent scope for the synthesis of a crystalline porous organic salt, enabling the discovery of a new porous salt (Fig. 30).[218] The screening was conducted using a Chemspeed Technologies AG Swing Powerdose robotic platform equipped with both solid and liquid dispensing tools, aiming to identify the optimal crystallisation conditions using increased concentrations and controlled addition of the solutions. Crystallisation was observed across 19 different crystallisation conditions (Fig. 30d), with the combination of EtOH and dioxane seemingly most suitable; THF also gave single crystals, albeit at the point of saturation, which was ultimately preferred for the scale up of the reaction to aid in solvent removal.

Further optimisation of the crystallisation was conducted using flow chemistry to enable the use of the desired non-polar solvents; saturated THF, at room temperature, was carried forward for the crystallisation of the salt, due to the ease with

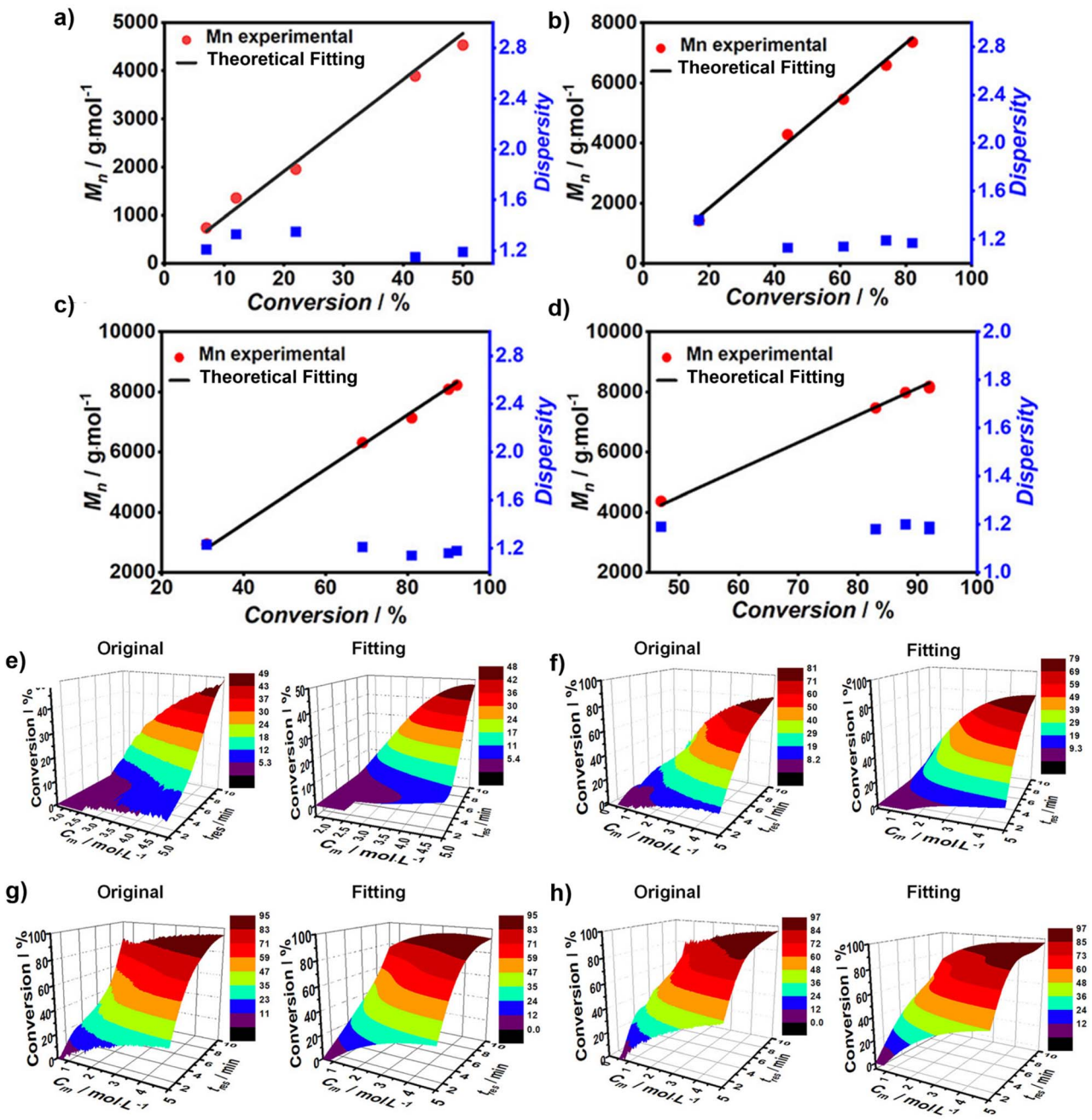

Fig. 33 Conversion of MA samples collected at the end of concentration-sweep experiments with different residence times (1, 3, 5, 8 and 10 minutes) analysed *via* inline FT-IR and high field NMR at (a) 80 °C, (b) 90 °C, (c) 100 °C, and (d) 110 °C. The initial concentration of MA for all the samples is 5 M. 3-Dimensional kinetic profiles of RAFT polymerisation of MA and their 3rd degree polynomial fitting at (e) 80 °C, (f) 90 °C, (g) 100 °C, and (h) 110 °C – copyright © 2023 Wiley. Used with permission from Zhang *et al.*[221] High throughput multidimensional kinetic screening in continuous flow reactors, *Angewandte Chemie International Edition* published by Wiley VCH Verlag GmbH.

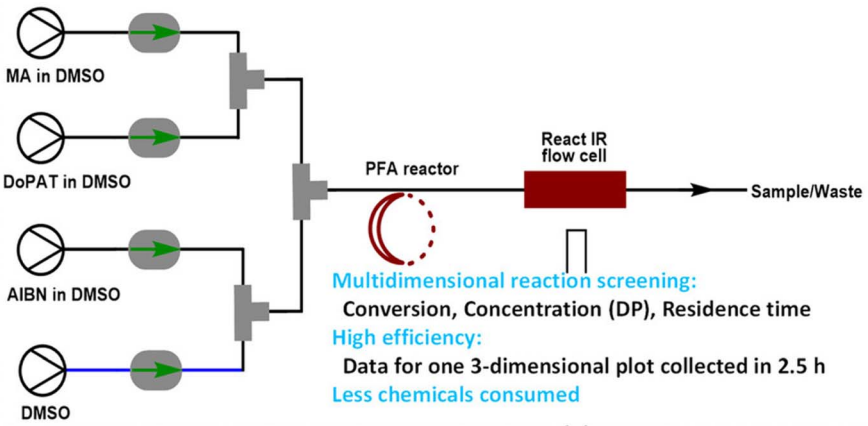

Fig. 34 Schematic outline of the continuous flow platform for the multidimensional kinetic screening of polymerisation reactions – copyright © 2023 Wiley. Used with permission from Zhang *et al.*[221] High throughput multidimensional kinetic screening in continuous flow reactors, *Angewandte Chemie International Edition* published by Wiley VCH Verlag GmbH.

which it can be removed compared to EtOH/dioxane. A dual syringe pump was initially used to deliver the two solutions, investigating the relationship between the quality of salt formation and the crystallisation time (residence time), with total flow rates ranging from 0.1–1.0 mL min^{-1}. Once optimal conditions had been established, the process was transferred to a Vapourtec Ltd E-series flow reactor, using a flow rate of 1.0 mL min^{-1} and a residence time of 35 seconds to obtain 150 mg of the desired salt – a productivity of 45 mg h^{-1} (Fig. 30b). The obtained material had significantly higher levels of crystallinity compared to the large-scale batch procedure (Fig. 30c) and was comparable to the small-scale optimised batch conditions of EtOH/dioxane.

In polymer synthesis, Judzewitsch *et al.* demonstrated the use of high throughput screening for the discovery of new antimicrobial polymers.[219] Similar to many of the examples of HTE in materials and supramolecular chemistry, the screening was conducted on a small-scale plate-based platform, with subsequent scale up facilitated by flow chemistry (Fig. 31). A series of cationic, hydrophilic, and hydrophobic monomers were screened using a 96-well microtiter plate; following 12 hours of irradiation under green light, the subsequent polymers were analysed *via* ^{1}H NMR. Following identification of the most promising polymers from this screening, structure–property relationships were analysed using a comparable batch plate-based approach, *via* compositional drift analysis and investigation of the repeat unit incorporation with time. A further compositional drift study was then conducted in flow using a 27 mL fluorinated ethylene propylene tubular photoreactor, operated under a slug flow regime, which was comparable to the previous plate results. A higher apparent rate of polymerisation in flow was noted, which was attributed to the improved irradiation efficiency and fluid circulation within the reaction slugs. The antimicrobial activity was also comparable for samples across the two techniques. This approach was scaled using flow to a throughput of 27.2 g per day, with the capability to scale up further *via* parallelisation.

Rubens *et al.* also reported a platform for polymer synthesis,[220] using a self-optimising flow reactor for the high-throughput screening and autonomous optimisation of polymerisation. The platform consisted of an online size exclusion chromatography system equipped with an evaporative light scattering detector, coupled to a flow polymerisation reactor (Fig. 32). Initial screening was conducted using the system targeting 20, 30, 40 and 50 degrees of polymerisation (DP), a metric for the number of monomer units in a polymer chain, with preset residence times for each DP. A feedback loop was then established that used an optimisation algorithm, with a user identified optimisation parameter selected prior to commencing a run. The system could be optimised for number average, weight average, or peak molecular weight. The platform showed widespread utility, successfully synthesising polymers across a range of molecular weights *via* the use of both a thermal and photo reactor. The platform could also be switched to a "process control mode" in which the system could be operated over an extended run time, with the algorithm adjusting as the run progressed to maintain the steady state and consistent output.

Within the same group, Zhang *et al.* published a high-throughput platform for conducting kinetic screening of polymerisation reactions in flow.[221] Inline FT-IR spectroscopy was employed for analysis, providing high temporal resolution for reactions whilst avoiding influence from the actual flow rate of the reactor. The platform was experimentally validated using a reversible addition–fragmentation chain transfer (RAFT) polymerisation reaction, with continuous variations of concentration achieved *via* alteration of the flow rate. A RAFT agent of 2-(dodecyl thiocarbonothioylthio)-propionic acid was used, with the monomer methyl acrylate (MA), and azobisisobutyronitrile as the thermal initiator. The monomer concentration gradient was altered from 0.5 M to 5 M throughout the experiment, whilst the RAFT agent concentration was kept constant. Three Python-controlled syringe pumps were used to deliver stock solutions of the reaction constituents, with

monomer concentration calculated from FT-IR spectra – all performance metrics indicated a high degree of accuracy between the programmed and measured concentrations.

Following validation, the polymerisation reaction was explored across a range of temperatures (80–110 °C) and residence times (1–10 minutes), automated using Python scripts. Samples of reaction mixture were collected from the concentration sweep experiment and analysed off-line *via* high-field NMR to cross reference the online data. Conversion ranged from 7–92% across the tested conditions, with longer residence times and higher temperature corresponding to higher conversions. The approach also proved highly reproducible, with 0.5% variance in monomer conversion observed for duplicated experiments, and a good agreement between the offline and online analysis was also observed with a 4% deviation between the two techniques. 3-D surface plots were then generated from the experimental data, from 2.5 hours of reaction time, with 3600 individual data points (Fig. 33) – it was noted that a similar volume of data would take up to 288 hours to collect by a conventional batch method. Polynomial fitting was also carried out to obtain a functional expression of the data, enabling subsequent prediction of experimental outcomes

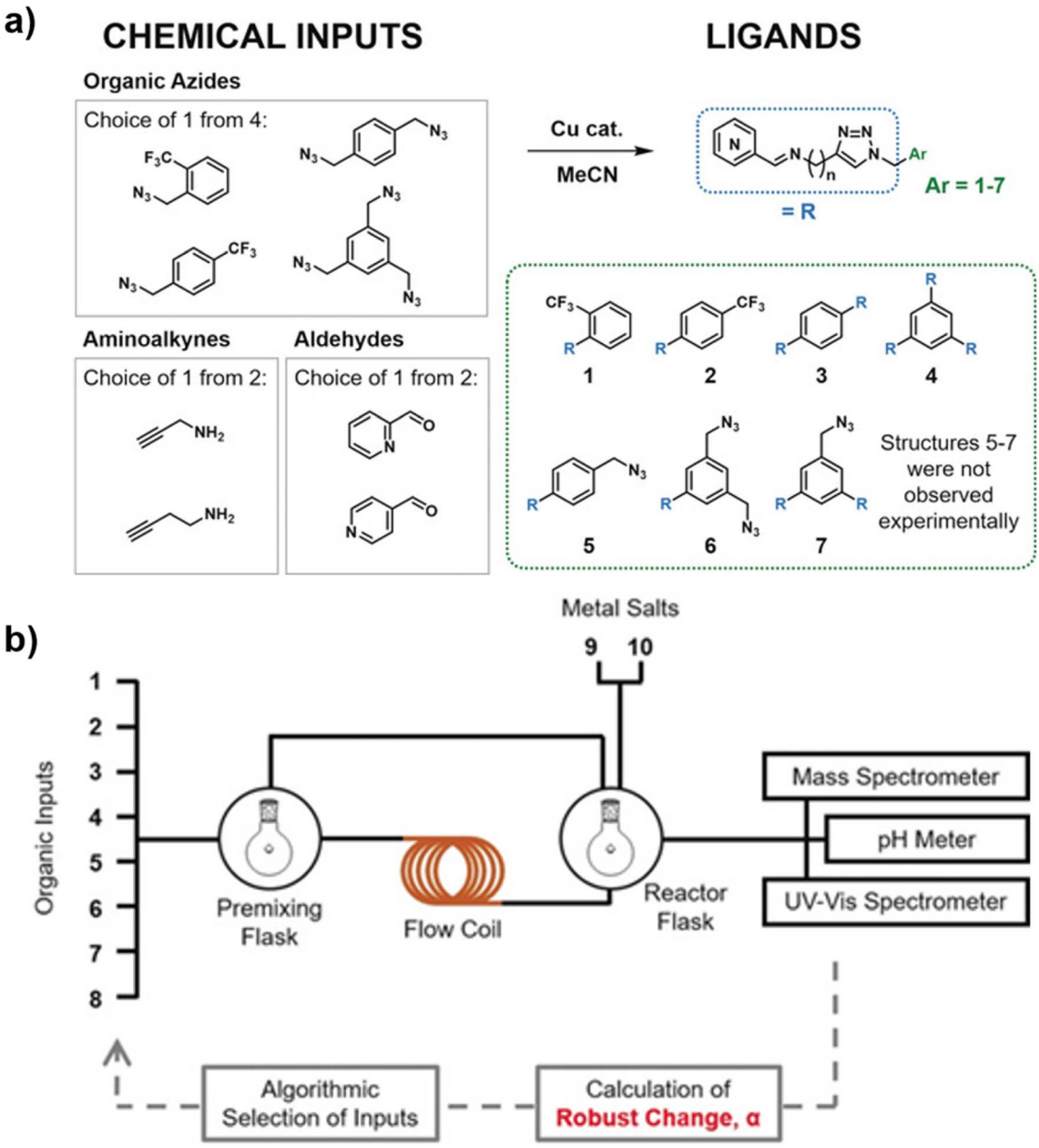

Fig. 35 (a) Small organic molecules used as chemical inputs for the synthesis of ligands, *via* tandem copper-catalyzed azide–alkyne cycloaddition and imine formation reactions, prior to complexation and (b) connection diagram of the system outlined – reproduced from Porwol *et al.*[222] with permission under the Creative Commons Attribution license (CC-BY). Copyright © 2020 Porwol *et al.*,[222] published by Wiley VCH Verlag GmbH & Co KGaA.

as a function of concentration and reaction time. The accuracy of the model was illustrated with an absolute error of 4.1% being observed between the predicted and experimental conversion.

The scope of the methodology was further expanded to include the screening of the degrees of polymerisation as a fourth screening dimension. To achieve this, the RAFT agent to monomer ratio was altered continuously *via* the introduction of a fourth syringe pump, to deliver each stock solution separately (Fig. 34). A DP gradient ranging from 50 to 170 was generated whilst maintaining the monomer concentration at 3 M and temperature at 110 °C. Analysis was conducted as per the previous experiment resulting in the generation of 3D surface plots for the monomer conversion, DP and residence time. A good polynomial fit was obtained with an r^2 value of 0.997, allowing comparison of the reaction rate with increasing DP. The method provided more detailed reaction metrics and insights than are usually afforded by comparative methods, which can be leveraged in target-oriented synthesis as the methodology provides users with the information required to make informed decisions required to generate targets of interest. Zhang *et al.* also highlighted that the methodology can be applied to a broader selection of reaction classes through the screening of a ring opening metathesis polymerisation.

Using an algorithmic approach, Porwol *et al.* reported a method for the discovery of supramolecular architectures (Fig. 35).[222] An exploration focused algorithm was used in a closed loop system to study the various combinations of one aldehyde, one amine, and one azide, in the presence of copper or cobalt (Fig. 35a). A screening of a range of conditions was conducted: various volumes, ratios, reaction times, and temperatures were explored, with reactivity determined *via* a combination of pH, and UV-vis and mass spectrometry. The platform was controlled *via* Python code and consisted of a chemical robot with liquid handling capabilities allowing the system to operate in a fully autonomous manner (Fig. 35b). From this screening, four novel coordinated structures were discovered and isolated, with their molecular structures determined *via* X-ray diffraction, illustrating the truly wide breadth of chemistry that can be efficiently explored using HTE and flow technologies.

The increased adoption of HTE across both supramolecular and materials chemistry has enabled the discovery of materials and the investigation of their corresponding properties, within increasingly shorter time frames. More widespread adoption of HTE in flow, within the two fields, is likely to further expedite the discovery and investigation of a broader range of materials in the coming years.

Conclusion and future perspectives

The benefits of flow in combination with HTE, including dynamic alteration of continuous variables, simplified scale up, improved heat and mass transfer, improved process window/safety and the ability to integrate PAT tools, are apparent from the case studies outlined in this review. Despite a widespread adoption of HTE in flow within certain fields, there are others that could benefit from increased adoption, particularly across both materials/supramolecular chemistry and organic methodology development where there is a distinct underutilisation. The future possibilities and opportunities for such technology are broad: the ability to pair the efficiency of HTE with the improved process control of flow chemistry offers opportunities to increase the efficacy of reaction discovery, optimisation and scale up. Adopting and adapting ideas and approaches from other chemical disciplines could enable more efficient and wide-reaching screening of both synthesis and property investigations. And as both HTE and flow chemistry are now considered mature technologies, with an increasing number of chemists becoming trained to use them, it seems likely that their use will proliferate, reducing material consumption and improving throughput, and ultimately accelerating reaction discovery and optimisation.

Thus far, much of the attention surrounding HTE has been centred around addressing chemistry- and engineering-focused challenges, such as handling volatile solvents, scaling up reactions, and improving reproducibility. However, some fundamental challenges remain – for example, the improved integration and efficacy of relevant in-line analytical techniques, telescoping flow HTE workflows into larger multistep processes, the translation from batch HTE to flow HTE, the use of heterogeneous mixtures, and the standardisation of equipment and procedures to enable meaningful comparisons between approaches.

Some of the studies outlined herein have attempted to tackle the challenge of translation, avoiding significant manual intervention and re-optimisation, but no universal solution has been found to date. The adoption of droplet microfluidic HTE platforms has gone some way to negate the issue, but platform development is not trivial, with specialist equipment and expertise often required. The same can be said for the challenge of heterogeneous chemistries, where the use of solid reagents in flow can lead to complications. The use of immobilised reagents within packed bed reactors somewhat addresses this challenge, although the utility of this approach in HTE platforms is hindered by degradation and loss of activity over time.

Further scope for improvements to HTE platforms also remain in the form of increased adoption of computational approaches, such as algorithmic optimisation, scheduling software and computer-aided planning tools. The rise of digitalisation and automation within chemistry, paired with the increasing prevalence of algorithmic/machine learning approaches, should enable technological leaps forward in the coming years. The large data sets generated by HTE activities are primed to train such models, enabling more accurate reflections of complex reaction methodologies, in addition to providing the much-needed negative data rarely found in publications.

Even as the technology becomes more widespread, a barrier to entry still exists in the form of access to skills, training, and equipment. Multidisciplinary teams with a diverse range of skills are often needed: the expertise of chemists, engineers and computer scientists/mathematicians may all be required. Educational tools are also sparse, as although many digital/flow

focused workshops are currently available for chemists, these typically lack the inclusion of the complementary skills required for HTE in flow. Additionally, if such training is available, it is typically only accessible to postgraduate or postdoctoral researchers, preventing students from developing all the required skills early in their education.

The cost associated with accessing the equipment and instrumentation required is also often prohibitively high. Various pieces of equipment with high associated costs are often used in tandem, pricing many academic and industrial groups/companies out of incorporating such approaches – although low-cost automation approaches are becoming more common.[223–226] It is hoped that with the continued, more widespread adoption of both flow chemistry and HTE, the required equipment will both reduce in cost and become more widely available, lowering the barrier to entry for the approach and encouraging more widespread adoption across all chemical fields.

Data availability

No primary research results, software or code has been included, and no new data was generated or analysed as part of this review.

Author contributions

George Lyall-Brookes: conceptualization, writing – original draft, writing – review & editing, visualisation. Alex C. Padgham: writing – review & editing, visualisation. Anna G. Slater: writing – review & editing, supervision, funding acquisition.

Conflicts of interest

The authors declare that they have no known competing financial interests or personal relationships that could have appeared to influence the work reported in this paper.

Acknowledgements

GLB thanks the Centre for Doctoral Training in Digital and Automated Materials Chemistry (EP/Y03502X/1) for funding that supported this work. AGS thanks the Royal Society for a University Research Fellowship (URF\R1\201168) that supported this work.

References

1 K. D. Collins, T. Gensch and F. Glorius, *Nat. Chem.*, 2014, **6**, 859–871.
2 M. S. Fogel and K. Koide, *Org. Process Res. Dev.*, 2023, **27**, 1235–1247.
3 D. K. B. Mohamed, X. Yu, J. Li and J. Wu, *Tetrahedron Lett.*, 2016, **57**, 3965–3977.
4 N. Yazdanpanah, C. N. Cruz and T. F. O'Connor, *Comput. Chem. Eng.*, 2019, **129**, 106510.
5 F. C. Whitmore and H. S. Rothrock, *J. Am. Chem. Soc.*, 1932, **54**, 3431–3435.
6 I. R. Baxendale, *J. Chem. Technol. Biotechnol.*, 2013, **88**, 519–552.
7 M. Guidi, P. H. Seeberger and K. Gilmore, *Chem. Soc. Rev.*, 2020, **49**, 8910–8932.
8 B. Gutmann and C. O. Kappe, *J. Flow Chem.*, 2017, **7**, 65–71.
9 A. Bonner, A. Loftus, A. C. Padgham and M. Baumann, *Org. Biomol. Chem.*, 2021, **19**, 7737–7753.
10 M. Power, E. Alcock and G. P. McGlacken, *Org. Process Res. Dev.*, 2020, **24**, 1814–1838.
11 S. P. Green, H. C. Broderick, K. M. P. Wheelhouse, J. P. Hallett, P. W. Miller and J. A. Bull, *J. Flow Chem.*, 2024, **14**, 559–568.
12 H. Lehmann, T. Ruppen and T. Knoepfel, *Org. Process Res. Dev.*, 2022, **26**, 1308–1317.
13 C. R. Sagandira and P. Watts, *Beilstein J. Org. Chem.*, 2019, **15**, 2577–2589.
14 P. Sagmeister, D. Kaldre, J. Sedelmeier, C. Moessner, K. Püntener, D. Kummli, J. D. Williams and C. O. Kappe, *Org. Process Res. Dev.*, 2021, **25**, 1206–1214.
15 K. S. O'Callaghan, D. Lynch, M. Baumann, S. G. Collins and A. R. Maguire, *Org. Biomol. Chem.*, 2023, **21**, 4770–4780.
16 L. Vinet, E. M. D. Allouche, V. Kairouz and A. B. Charette, *J. Flow Chem.*, 2024, **14**, 109–118.
17 F. M. Akwi and P. Watts, *Chem. Commun.*, 2018, **54**, 13894–13928.
18 A. Slattery, Z. Wen, P. Tenblad, J. Sanjosé-Orduna, D. Pintossi, T. den Hartog and T. Noël, *Science*, 2024, **383**, eadj1817.
19 D. Karan, G. Chen, N. Jose, J. Bai, P. McDaid and A. A. Lapkin, *React. Chem. Eng.*, 2024, **9**, 619–629.
20 A. D. Clayton, A. M. Schweidtmann, G. Clemens, J. A. Manson, C. J. Taylor, C. G. Niño, T. W. Chamberlain, N. Kapur, A. J. Blacker, A. A. Lapkin and R. A. Bourne, *Chem. Eng. J.*, 2020, **384**, 123340.
21 FlowCAT Platform, **https://helgroup.com/products/catalysis/flowcat/?srsltid=AfmBOor3JFP3buI6Uznn0YKz9MxsLIbbMvElTeWIX0m6RfyyfWZ3V9CZ**, accessed June 2025.
22 Vapourtec R-series, **https://www.vapourtec.com/products/r-series-flow-chemistry-system-overview/**, accessed June 2025.
23 Asia Premium Flow Chemistry System, **https://www.syrris.com/product/asia-premium-flow-chemistry-system/**, accessed June 2025.
24 Uniqsis FlowSyn, **https://www.uniqsis.com/paProductsDetail.aspx?ID=FLW_SYN**, accessed June 2025.
25 J. Wu, X. Yang, Y. Pan, T. Zuo, Z. Ning, C. Li and Z. Zhang, *J. Flow Chem.*, 2023, **13**, 385–404.
26 A. D. Clayton, *Chem. Methods*, 2023, **3**, e202300021.
27 J. P. McMullen and B. M. Wyvratt, *React. Chem. Eng.*, 2023, **8**, 137–151.
28 S. L. Boyall, H. Clarke, T. Dixon, R. W. M. Davidson, K. Leslie, G. Clemens, F. L. Muller, A. D. Clayton, R. A. Bourne and T. W. Chamberlain, *ACS Sustain. Chem. Eng.*, 2024, **12**, 15125–15133.

29 Y. Wang, J. Li, X. Chen, W. Zhu, X. Guo and F. Zhao, *Artif. Intell. Chem.*, 2024, **2**, 100066.
30 C. J. Taylor, J. A. Manson, G. Clemens, B. A. Taylor, T. W. Chamberlain and R. A. Bourne, *React. Chem. Eng.*, 2022, **7**, 1037–1046.
31 E. Agunloye, P. Petsagkourakis, M. Yusuf, R. Labes, T. Chamberlain, F. L. Muller, R. A. Bourne and F. Galvanin, *React. Chem. Eng.*, 2024, **9**, 1859–1876.
32 P. Jankowski, R. Kutaszewicz, D. Ogończyk and P. Garstecki, *J. Flow Chem.*, 2020, **10**, 397–408.
33 W. F. Maier, *ACS Comb. Sci.*, 2019, **21**, 437–444.
34 S. W. Krska, D. A. DiRocco, S. D. Dreher and M. Shevlin, *Acc. Chem. Res.*, 2017, **50**, 2976–2985.
35 A. B. Santanilla and G. Cook, in *The Power of High-Throughput Experimentation: Case Studies from Drug Discovery, Drug Development, and Catalyst Discovery*, ed. M. H. Emmert, M. Jouffroy and D. C. Leitch, American Chemical Society, Washington D. C., 2022, vol. 2, ch. 1, pp. 3–21.
36 M. Shevlin, *ACS Med. Chem. Lett.*, 2017, **8**, 601–607.
37 M. N. Bahr, D. B. Damon, S. D. Yates, A. S. Chin, J. D. Christopher, S. Cromer, N. Perrotto, J. Quiroz and V. Rosso, *Org. Process Res. Dev.*, 2018, **22**, 1500–1508.
38 K. Olsen, *SLAS Technol.*, 2012, **17**(6), 469–480.
39 J. Schuster, V. Kamuju, J. Zhou and R. Mathaes, *SLAS Technol.*, 2024, **29**(3), 100128.
40 D. A. Pereira and J. A. Wiliams, *Br. J. Pharmacol.*, 2007, **152**, 53–61.
41 A.-K. Becker, H. Erfle, M. Gunkel, N. Beil, L. Kaderali and V. Starkuviene, *High-Throughput*, 2018, **7**, 13.
42 X. Caldentey and E. Romero, *Chem. Methods*, 2023, **3**, e202200059.
43 M. H. Reis, C. L. G. Davidson and F. A. Leibfarth, *Polym. Chem.*, 2018, **9**, 1728–1734.
44 A. Buitrago Santanilla, E. L. Regalado, T. Pereira, M. Shevlin, K. Bateman, L.-C. Campeau, J. Schneeweis, S. Berritt, Z.-C. Shi, P. Nantermet, Y. Liu, R. Helmy, C. J. Welch, P. Vachal, I. W. Davies, T. Cernak and S. D. Dreher, *Science*, 2015, **347**, 49–53.
45 J. Yu, J. Liu, C. Li, J. Huang, Y. Zhu and H. You, *Chem. Commun.*, 2024, **60**, 3217–3225.
46 J. Mason, H. Wilders, D. J. Fallon, R. P. Thomas, J. T. Bush, N. C. O. Tomkinson and F. Rianjongdee, *Digital Discovery*, 2023, **2**, 1894–1899.
47 J. W. Sawicki, A. R. Bogdan, P. A. Searle, N. Talaty and S. W. Djuric, *React. Chem. Eng.*, 2019, **4**, 1589–1594.
48 S. M. Mennen, C. Alhambra, C. L. Allen, M. Barberis, S. Berritt, T. A. Brandt, A. D. Campbell, J. Castañón, A. H. Cherney, M. Christensen, D. B. Damon, J. Eugenio de Diego, S. García-Cerrada, P. García-Losada, R. Haro, J. Janey, D. C. Leitch, L. Li, F. Liu, P. C. Lobben, D. W. C. MacMillan, J. Magano, E. McInturff, S. Monfette, R. J. Post, D. Schultz, B. J. Sitter, J. M. Stevens, I. I. Strambeanu, J. Twilton, K. Wang and M. A. Zajac, *Org. Process Res. Dev.*, 2019, **23**, 1213–1242.
49 B. Mahjour, Y. Shen and T. Cernak, *Acc. Chem. Res.*, 2021, **54**, 2337–2346.
50 C. B. Berlin, H. F. Roenfanz, M. Salwen, S. Nehete and M. C. Kozlowski, *Org. Lett.*, 2024, **26**, 5243–5247.
51 M. González-Esguevillas, D. F. Fernández, J. A. Rincón, M. Barberis, O. de Frutos, C. Mateos, S. García-Cerrada, J. Agejas and D. W. C. MacMillan, *ACS Cent. Sci.*, 2021, **7**, 1126–1134.
52 J. D. Williams and C. O. Kappe, *Curr. Opin. Green Sustainable Chem.*, 2020, **25**, 100351.
53 C. Sambiagio and T. Noël, *Trends Chem.*, 2020, **2**, 92–106.
54 K. Donnelly and M. Baumann, *J. Flow Chem.*, 2021, **11**, 223–241.
55 D. Cambié, C. Bottecchia, N. J. W. Straathof, V. Hessel and T. Noël, *Chem. Rev.*, 2016, **116**, 10276–10341.
56 Corning Photoreactor, **https://www.corning.com/media/worldwide/global/documents/PhotoReactor.leaflet_FINAL_5.18.15.pdf**, accessed June 2025.
57 Vapourtec UV150 Photoreactor, **https://www.vapourtec.com/products/flow-reactors/photochemical-reactor-uv-150-features/**, accessed June 2025.
58 Uniqsis Photosyn, **https://www.uniqsis.com/paProductsDetail.aspx?ID=PhotoSyn**, accessed June 2025.
59 Syrris Photoreactor, **https://www.syrris.com/product/asia-photochemistry-system/?creative=583921274148&keyword=flowphotochemicalreactor&matchtype=p&network=g&device=c&gad_source=**, accessed June 2025.
60 D. Cantillo, O. de Frutos, J. A. Rincon, C. Mateos and C. O. Kappe, *J. Org. Chem.*, 2014, **79**, 223–229.
61 D. Cambié, F. Zhao, V. Hessel, M. G. Debije and T. Noël, *Angew. Chem., Int. Ed.*, 2017, **56**, 1050–1054.
62 B. D. Hook, W. Dohle, P. R. Hirst, M. Pickworth, M. B. Berry and K. I. Booker-Milburn, *J. Org. Chem.*, 2005, **70**, 7558–7564.
63 Acceled Photoreactor m2, **https://www.acceledbio.com/photoreactor-m2**, accessed June 2025.
64 Lumidox II LED, **https://www.analytical-sales.com/product-category/photoredox-parallel-synthesis/lumidox-ii-led-arrays-lamps/?gad_source=1&gclid=Cj0KCQjwsJO4BhDoARIsADDv4vCv-N2G3wPY0z6HCh-kPQzzBqBYqKNtDFFUUzymBcAXD2R1eIbaYI4aAocCEALw_wcB**, accessed June 2025.
65 Luzchem Well Plate Illuminator, **https://luzchem.com/products/well-plate-illuminator?srsltid=AfmBOoqdHbRHFe89KHDRu3d_mPPQtNItAoQ-B0QQYYj_7QWeDCqDdyaO**, accessed June 2025.
66 SynLED Parallel Photoreactor, **https://www.sigmaaldrich.com/deepweb/assets/sigmaaldrich/product/documents/398/704/z742680bul.pdf**, accessed June 2025.
67 EvoluChem PhotoRedOx Box TC™, **https://hepatochem.com/photoreactors-leds-accessories/photoredox-temperature-controlled/**, accessed June 2025.
68 Lumidox®II 48-Position LED Array, **https://www.analytical-sales.com/product/lumidoxii-48-position-led-arrays-for-tcr/**

?srsltid=AfmBOooPVi-8DNNbW40SeZLioizrO_Z1yiukyVaLFgIt9XgkqyXanvGn, accessed June 2025.
69 TREX photoreactor, http://treellumtechnologies.com/#products, accessed June 2025.
70 Lumidox Gen2 96-Well LED Array, https://www.analytical-sales.com/brochure/lumidox_ll_96-well_arrays_rev1d.pdf?srsltid=AfmBOoqzv3TY4KWEe50kKiMQi63tSpiRGxxKZW4jurRg_ZzSeBVI9kRh, accessed June 2025.
71 T. Jerkovic, H. Cruickshank, Y. Chen, A. F. Trindade, A. M. Dumas, J. Edwards, A. Alorati and H. E. Ho, *Org. Process Res. Dev.*, 2024, **28**, 266–272.
72 TAK120 LC, http://photoreactor.de/, accessed June 2025.
73 S. A. Weissman and N. G. Anderson, *Org. Process Res. Dev.*, 2015, **19**, 1605–1633.
74 Y. Mori, M. Hayashi, R. Sato, K. Tai and T. Nagase, *Org. Lett.*, 2023, **25**, 5569–5573.
75 A. C. Sun, D. J. Steyer, A. R. Allen, E. M. Payne, R. T. Kennedy and C. R. J. Stephenson, *Nat. Commun.*, 2020, **11**, 6202.
76 B. Pijper, L. M. Saavedra, M. Lanzi, M. Alonso, A. Fontana, M. Serrano, J. E. Gómez, A. W. Kleij, J. Alcázar and S. Cañellas, *JACS Au*, 2024, **4**, 2585–2595.
77 F. Wagner, P. Sagmeister, C. E. Jusner, T. G. Tampone, V. Manee, F. G. Buono, J. D. Williams and C. O. Kappe, *Adv. Sci.*, 2024, **11**, 2308034.
78 A. C. Sun, D. J. Steyer, R. I. Robinson, C. Ginsburg-Moraff, S. Plummer, J. Gao, J. W. Tucker, D. Alpers, C. R. J. Stephenson and R. T. Kennedy, *Angew. Chem., Int. Ed.*, 2023, **62**, e202301664.
79 S. Chatterjee, M. Guidi, P. H. Seeberger and K. Gilmore, *Nature*, 2020, **579**, 379–384.
80 H.-W. Hsieh, C. W. Coley, L. M. Baumgartner, K. F. Jensen and R. I. Robinson, *Org. Process Res. Dev.*, 2018, **22**, 542–550.
81 J. J. Mousseau, M. A. Perry, M. W. Bundesmann, G. M. Chinigo, C. Choi, G. Gallego, R. W. Hicklin, S. Hoy, D. C. Limburg, N. W. Sach and Y. Zhang, *ACS Catal.*, 2022, **12**, 600–606.
82 B. Pijper, I. Abdiaj, D. Leonori and J. Alcázar, *ChemCatChem*, 2023, **15**, e202201289.
83 Z. Arshad, A. J. Blacker, T. W. Chamberlain, N. Kapur, A. D. Clayton and R. A. Bourne, *Curr. Opin. Green Sustainable Chem.*, 2024, **48**, 100940.
84 Z. Peng, G. Wang, B. Moghtaderi and E. Doroodchi, *Chem. Eng. Sci.*, 2022, **247**, 117040.
85 J. W. Beatty, J. J. Douglas, K. P. Cole and C. R. J. Stephenson, *Nat. Commun.*, 2015, **6**, 7919.
86 S. Sun, T. R. Slaney and R. T. Kennedy, *Anal. Chem.*, 2012, **84**, 5794–5800.
87 S. Sun and R. T. Kennedy, *Anal. Chem.*, 2014, **86**, 9309–9314.
88 X. W. Diefenbach, I. Farasat, E. D. Guetschow, C. J. Welch, R. T. Kennedy, S. Sun and J. C. Moore, *ACS Omega*, 2018, **3**, 1498–1508.
89 D. J. Steyer and R. T. Kennedy, *Anal. Chem.*, 2019, **91**, 6645–6651.
90 Y.-J. Hwang, C. W. Coley, M. Abolhasani, A. L. Marzinzik, G. Koch, C. Spanka, H. Lehmann and K. F. Jensen, *Chem. Commun.*, 2017, **53**, 6649–6652.
91 M. Abolhasani, N. C. Bruno and K. F. Jensen, *Chem. Commun.*, 2015, **51**, 8916–8919.
92 R. C. McAtee, J. W. Beatty, C. C. McAtee and C. R. J. Stephenson, *Org. Lett.*, 2018, **20**, 3491–3495.
93 A. C. Sun, E. J. McClain, J. W. Beatty and C. R. J. Stephenson, *Org. Lett.*, 2018, **20**, 3487–3490.
94 C. J. Taylor, A. Pomberger, K. C. Felton, R. Grainger, M. Barecka, T. W. Chamberlain, R. A. Bourne, C. N. Johnson and A. A. Lapkin, *Chem. Rev.*, 2023, **123**, 3089–3126.
95 F. L. Wagner, P. Sagmeister, T. G. Tampone, V. Manee, D. Yerkozhanov, F. G. Buono, J. D. Williams and C. O. Kappe, *ACS Sustain. Chem. Eng.*, 2024, **12**, 10002–10010.
96 M. I. Jeraal, S. Sung and A. A. Lapkin, *Chem. Methods*, 2021, **1**, 71–77.
97 M. D. McKay, R. J. Beckman and W. J. Conover, *Technometrics*, 1979, **21**, 239–245.
98 R. T. Marler and J. S. Arora, *Struct. Multidiscip. Optim.*, 2010, **41**, 853–862.
99 B. P. MacLeod, F. G. L. Parlane, C. C. Rupnow, K. E. Dettelbach, M. S. Elliott, T. D. Morrissey, T. H. Haley, O. Proskurin, M. B. Rooney, N. Taherimakhsousi, D. J. Dvorak, H. N. Chiu, C. E. B. Waizenegger, K. Ocean, M. Mokhtari and C. P. Berlinguette, *Nat. Commun.*, 2022, **13**, 995.
100 K. Swersky, J. Snoek and R. P. Adams, *Advances in Neural Information Processing Systems*, 2013, vol. 26.
101 C. J. Taylor, K. C. Felton, D. Wigh, M. I. Jeraal, R. Grainger, G. Chessari, C. N. Johnson and A. A. Lapkin, *ACS Cent. Sci.*, 2023, **9**, 957–968.
102 P. Müller, A. D. Clayton, J. Manson, S. Riley, O. S. May, N. Govan, S. Notman, S. V. Ley, T. W. Chamberlain and R. A. Bourne, *React. Chem. Eng.*, 2022, **7**, 987–993.
103 K. C. Felton, J. G. Rittig and A. A. Lapkin, *Chem. Methods*, 2021, **1**, 116–122.
104 C. Avila, C. Cassani, T. Kogej, J. Mazuela, S. Sarda, A. D. Clayton, M. Kossenjans, C. P. Green and R. A. Bourne, *Chem. Sci.*, 2022, **13**, 12087–12099.
105 K. E. Konan, A. Senthil Vel, A. Abollé, D. Cortés-Borda and F.-X. Felpin, *React. Chem. Eng.*, 2023, **8**, 2446–2454.
106 R. P. Hsung, A. V. Kurdyumov and N. Sydorenko, *Eur. J. Org Chem.*, 2005, **2005**, 23–44.
107 A. V. Kurdyumov, N. Lin, R. P. Hsung, G. C. Gullickson, K. P. Cole, N. Sydorenko and J. J. Swidorski, *Org. Lett.*, 2006, **8**, 191–193.
108 J. Moreau, C. Hubert, J. Batany, L. Toupet, T. Roisnel, J.-P. Hurvois and J.-L. Renaud, *J. Org. Chem.*, 2009, **74**, 8963–8973.
109 A. D. Fotiadou and A. L. Zografos, *Org. Lett.*, 2012, **14**, 5664–5667.
110 D. Cortés-Borda, K. V. Kutonova, C. Jamet, M. E. Trusova, F. Zammattio, C. Truchet, M. Rodriguez-Zubiri and F.-X. Felpin, *Org. Process Res. Dev.*, 2016, **20**, 1979–1987.

111 N. S. Eyke, T. N. Schneider, B. Jin, T. Hart, S. Monfette, J. M. Hawkins, P. D. Morse, R. M. Howard, D. M. Pfisterer, K. Y. Nandiwale and K. F. Jensen, *Chem. Sci.*, 2023, **14**, 8798–8809.
112 I. W. Ashworth, L. Frodsham, P. Moore and T. O. Ronson, *J. Org. Chem.*, 2022, **87**, 2111–2119.
113 N. Guha, V. Baladandayuthapani and B. K. Mallick, *J. Mach. Learn. Res.*, 2020, **21**, 1–47.
114 F. Florit, K. Y. Nandiwale, C. T. Armstrong, K. Grohowalski, A. R. Diaz, J. Mustakis, S. M. Guinness and K. F. Jensen, *React. Chem. Eng.*, 2025, **10**, 656–666.
115 I. Averbakh, *Discrete Optim.*, 2005, **2**, 273–287.
116 N. S. Eyke, B. A. Koscher and K. F. Jensen, *Trends Chem.*, 2021, **3**, 120–132.
117 J. P. Edaugal, D. Zhang, D. Liu, V.-A. Glezakou and N. Sun, *Chem Bio Eng.*, 2025, **2**, 210–228.
118 A. Nandy, C. Duan, M. G. Taylor, F. Liu, A. H. Steeves and H. J. Kulik, *Chem. Rev.*, 2021, **121**, 9927–10000.
119 K. McCullough, T. Williams, K. Mingle, P. Jamshidi and J. Lauterbach, *Phys. Chem. Chem. Phys.*, 2020, **22**, 11174–11196.
120 A. R. Rosales, J. Wahlers, E. Limé, R. E. Meadows, K. W. Leslie, R. Savin, F. Bell, E. Hansen, P. Helquist, R. H. Munday, O. Wiest and P.-O. Norrby, *Nat. Catal.*, 2019, **2**, 41–45.
121 T. Stuyver and C. W. Coley, *Chem.–Eur. J.*, 2023, **29**, e202300387.
122 C. W. Coley, D. A. Thomas, J. A. M. Lummiss, J. N. Jaworski, C. P. Breen, V. Schultz, T. Hart, J. S. Fishman, L. Rogers, H. Gao, R. W. Hicklin, P. P. Plehiers, J. Byington, J. S. Piotti, W. H. Green, A. J. Hart, T. F. Jamison and K. F. Jensen, *Science*, 2019, **365**, eaax1566.
123 A. M. K. Nambiar, C. P. Breen, T. Hart, T. Kulesza, T. F. Jamison and K. F. Jensen, *ACS Cent. Sci.*, 2022, **8**, 825–836.
124 A. M. Armaly, Y. C. DePorre, E. J. Groso, P. S. Riehl and C. S. Schindler, *Chem. Rev.*, 2015, **115**, 9232–9276.
125 M. Heravi and V. Zadsirjan, *Recent Advances in Applications of Name Reactions in Multicomponent Reactions*, Elsevier, Amsterdam, 2020.
126 C. J. Gerry and S. L. Schreiber, *Nat. Rev. Drug Discovery*, 2018, **17**, 333–352.
127 S. A. Biyani, Y. W. Moriuchi and D. H. Thompson, *Chem. Methods*, 2021, **1**, 323–339.
128 E. S. Isbrandt, R. J. Sullivan and S. G. Newman, *Angew. Chem., Int. Ed.*, 2019, **58**, 7180–7191.
129 M. Farhang, A. R. Akbarzadeh, M. Rabbani and A. M. Ghadiri, *Polyhedron*, 2022, **227**, 116124.
130 K. Masuda, T. Ichitsuka, N. Koumura, K. Sato and S. Kobayashi, *Tetrahedron*, 2018, **74**, 1705–1730.
131 H. Ishitani, Y. Saito, B. Laroche, X. Rao and S. Kobayashi, in *Flow Chemistry: Integrated Approaches for Practical Applications*, ed. S. V. Luis and E. Garcia-Verdugo, The Royal Society of Chemistry, London, 2019, vol. 1, pp. 1–49.
132 F. Lévesque, N. J. Rogus, G. Spencer, P. Grigorov, J. P. McMullen, D. A. Thaisrivongs, I. W. Davies and J. R. Naber, *Org. Process Res. Dev.*, 2018, **22**, 1015–1021.
133 I. S. Patel, G. Ganesan and S. Jain, *Org. Process Res. Dev.*, 2024, **28**, 3464–3508.
134 Z. Jaman, A. Mufti, S. Sah, L. Avramova and D. H. Thompson, *Chem.–Eur. J.*, 2018, **24**, 9546–9554.
135 B. J. Reizman, Y.-M. Wang, S. L. Buchwald and K. F. Jensen, *React. Chem. Eng.*, 2016, **1**, 658–666.
136 S. Kozuch and J. M. L. Martin, *ACS Catal.*, 2012, **2**, 2787–2794.
137 S. K. Kashani, J. E. Jessiman and S. G. Newman, *Org. Process Res. Dev.*, 2020, **24**, 1948–1954.
138 G. Lennon and P. Dingwall, *Angew. Chem., Int. Ed.*, 2024, **63**, e202318146.
139 D. G. Blackmond, *Angew. Chem., Int. Ed.*, 2005, **44**, 4302–4320.
140 J. Van Herck and T. Junkers, *Chem. Methods*, 2022, **2**, e202100090.
141 L. Schrecker, J. Dickhaut, C. Holtze, P. Staehle, A. Wieja, K. Hellgardt and K. K. Hii, *React. Chem. Eng.*, 2023, **8**, 3196–3202.
142 F. Vega-Ramon, L. Schrecker, M. A. de Carvalho Servia, K. K. M. Hii and D. Zhang, in *Computer Aided Chemical Engineering*, ed. F. Manenti and G. V. Reklaitis, Elsevier, 2024, vol. 53, pp. 55–60.
143 C. J. Taylor, M. Booth, J. A. Manson, M. J. Willis, G. Clemens, B. A. Taylor, T. W. Chamberlain and R. A. Bourne, *Chem. Eng. J.*, 2021, **413**, 127017.
144 K. C. Aroh and K. F. Jensen, *React. Chem. Eng.*, 2018, **3**, 94–101.
145 P. Sagmeister, L. Melnizky, J. D. Williams and C. O. Kappe, *Chem. Sci.*, 2024, **15**, 12523–12533.
146 B. List, R. A. Lerner and C. F. Barbas, *J. Am. Chem. Soc.*, 2000, **122**, 2395–2396.
147 N. Zotova, L. J. Broadbelt, A. Armstrong and D. G. Blackmond, *Bioorg. Med. Chem. Lett.*, 2009, **19**, 3934–3937.
148 N. Zotova, A. Franzke, A. Armstrong and D. G. Blackmond, *J. Am. Chem. Soc.*, 2007, **129**, 15100–15101.
149 M. J. Di Maso, J. T. Kuethe, K. Narsimhan, M. Burris, C. K. Chung, M. DiBenedetto, J. H. Forstater, S. T. Grosser, N. Kuhl, F. Lévesque, A. Maguire, K. M. Maloney, J. P. McMullen, C. K. Prier, J. Qi, N. R. Rivera, Z. Wang, B. M. Wyvratt and D. Zewge, *Org. Process Res. Dev.*, 2024, **28**, 1764–1772.
150 C. Costentin and J.-M. Savéant, *Proc. Natl. Acad. Sci. U. S. A.*, 2019, **116**, 11147–11152.
151 J. Lodh, S. Paul, H. Sun, L. Song, W. Schöfberger and S. Roy, *Front. Chem.*, 2022, **10**, 956502.
152 Z. J. Oliver, D. J. Abrams, L. Cardinale, C.-J. Chen, G. L. Beutner, S. Caille, B. Cohen, L. Deng, M. Diwan, M. O. Frederick, K. Harper, J. M. Hawkins, D. Lehnherr, C. Lucky, A. Meyer, S. Noh, D. Nunez, K. Quasdorf, J. Teli, S. S. Stahl and M. Schreier, *ACS Cent. Sci.*, 2025, **11**(4), 528–538.
153 A. G. Wills, S. Charvet, C. Battilocchio, C. C. Scarborough, K. M. P. Wheelhouse, D. L. Poole, N. Carson and J. C. Vantourout, *Org. Process Res. Dev.*, 2021, **25**, 2587–2600.

154 M. Regnier, C. Vega, D. I. Ioannou and T. Noël, *Chem. Soc. Rev.*, 2024, **53**, 10741–10760.
155 N. Tanbouza, T. Ollevier and K. Lam, *iScience*, 2020, **23**, 101720.
156 T. Noël, Y. Cao and G. Laudadio, *Acc. Chem. Res.*, 2019, **52**, 2858–2869.
157 C. Gütz, A. Stenglein and S. R. Waldvogel, *Org. Process Res. Dev.*, 2017, **21**, 771–778.
158 M. A. Kabeshov, B. Musio, P. R. D. Murray, D. L. Browne and S. V. Ley, *Org. Lett.*, 2014, **16**, 4618–4621.
159 R. A. Green, K. E. Jolley, A. A. M. Al-Hadedi, D. Pletcher, D. C. Harrowven, O. De Frutos, C. Mateos, D. J. Klauber, J. A. Rincón and R. C. D. Brown, *Org. Lett.*, 2017, **19**, 2050–2053.
160 R. Becker, K. Weber, T. V. Pfeiffer, J. v. Kranendonk and K. J. Schouten, *Catalysts*, 2020, **10**, 1165.
161 M. Lehmann, C. C. Scarborough, E. Godineau and C. Battilocchio, *Ind. Eng. Chem. Res.*, 2020, **59**, 7321–7326.
162 Y. Mo, G. Rughoobur, A. M. K. Nambiar, K. Zhang and K. F. Jensen, *Angew. Chem., Int. Ed.*, 2020, **59**, 20890–20894.
163 D. Pletcher, R. A. Green and R. C. D. Brown, *Chem. Rev.*, 2018, **118**, 4573–4591.
164 E. Rial-Rodríguez, J. F. Wagner, H.-M. Eggenweiler, T. Fuchss, A. Sommer, C. O. Kappe, J. D. Williams and D. Cantillo, *React. Chem. Eng.*, 2024, **9**, 31–36.
165 E. Rial-Rodríguez, J. D. Williams, D. Cantillo, T. Fuchß, A. Sommer, H.-M. Eggenweiler, C. O. Kappe and G. Laudadio, *Angew. Chem., Int. Ed.*, 2024, **63**, e202412045.
166 H.-J. Schäfer, in *Electrochemistry IV*, Springer, Berlin, 2005, pp. 91–151.
167 H. Hofer and M. Moest, *Adv. Cycloaddit.*, 1902, **323**, 284–323.
168 Y. Kawamata, J. C. Vantourout, D. P. Hickey, P. Bai, L. Chen, Q. Hou, W. Qiao, K. Barman, M. A. Edwards, A. F. Garrido-Castro, J. N. deGruyter, H. Nakamura, K. Knouse, C. Qin, K. J. Clay, D. Bao, C. Li, J. T. Starr, C. Garcia-Irizarry, N. Sach, H. S. White, M. Neurock, S. D. Minteer and P. S. Baran, *J. Am. Chem. Soc.*, 2019, **141**, 6392–6402.
169 C. Li, Y. Kawamata, H. Nakamura, J. C. Vantourout, Z. Liu, Q. Hou, D. Bao, J. T. Starr, J. Chen, M. Yan and P. S. Baran, *Angew. Chem., Int. Ed.*, 2017, **56**, 13088–13093.
170 J. Morvan, K. P. L. Kuijpers, D. Fanfair, B. Tang, K. Bartkowiak, L. van Eynde, E. Renders, J. Alcazar, P. Buijnsters, M. A. Carvalho and A. X. Jones, *Angew. Chem., Int. Ed.*, 2025, **64**, e202413383.
171 G. L. Patrick, *An Introduction to Medicinal Chemistry*, OUP, Oxford, 2023.
172 C. J. Manly, J. Chandrasekhar, J. W. Ochterski, J. D. Hammer and B. B. Warfield, *Drug Discovery Today*, 2008, **13**, 99–109.
173 I. B. Campbell, S. J. F. Macdonald and P. A. Procopiou, *Drug Discovery Today*, 2018, **23**, 219–234.
174 K. C. Nicolaou, *Angew. Chem., Int. Ed.*, 2014, **53**, 9128–9140.
175 D. Perera, J. W. Tucker, S. Brahmbhatt, C. J. Helal, A. Chong, W. Farrell, P. Richardson and N. W. Sach, *Science*, 2018, **359**, 429–434.
176 A. Günther and K. F. Jensen, *Lab Chip*, 2006, **6**, 1487–1503.
177 B. J. Reizman and K. F. Jensen, *Chem. Commun.*, 2015, **51**, 13290–13293.
178 N. Hawbaker, E. Wittgrove, B. Christensen, N. Sach and D. G. Blackmond, *Org. Process Res. Dev.*, 2016, **20**, 465–473.
179 J. Jover, N. Fey, J. N. Harvey, G. C. Lloyd-Jones, A. G. Orpen, G. J. J. Owen-Smith, P. Murray, D. R. J. Hose, R. Osborne and M. Purdie, *Organometallics*, 2012, **31**, 5302–5306.
180 J. Jover, N. Fey, J. N. Harvey, G. C. Lloyd-Jones, A. G. Orpen, G. J. J. Owen-Smith, P. Murray, D. R. J. Hose, R. Osborne and M. Purdie, *Organometallics*, 2010, **29**, 6245–6258.
181 P. G. Gildner and T. J. Colacot, *Organometallics*, 2015, **34**, 5497–5508.
182 P. M. Murray, F. Bellany, L. Benhamou, D.-K. Bučar, A. B. Tabor and T. D. Sheppard, *Org. Biomol. Chem.*, 2016, **14**, 2373–2384.
183 N. Schneider, D. M. Lowe, R. A. Sayle, M. A. Tarselli and G. A. Landrum, *J. Med. Chem.*, 2016, **59**, 4385–4402.
184 S. D. Roughley and A. M. Jordan, *J. Med. Chem.*, 2011, **54**, 3451–3479.
185 R. Hili and A. K. Yudin, *Nat. Chem. Biol.*, 2006, **2**, 284–287.
186 D. G. Brown and J. Boström, *J. Med. Chem.*, 2016, **59**, 4443–4458.
187 Z. Jaman, D. L. Logsdon, B. Szilágyi, T. J. P. Sobreira, D. Aremu, L. Avramova, R. G. Cooks and D. H. Thompson, *ACS Comb. Sci.*, 2020, **22**, 184–196.
188 M. Wleklinski, B. P. Loren, C. R. Ferreira, Z. Jaman, L. Avramova, T. J. P. Sobreira, D. H. Thompson and R. G. Cooks, *Chem. Sci.*, 2018, **9**, 1647–1653.
189 H. S. Ewan, S. A. Biyani, J. DiDomenico, D. Logsdon, T. J. P. Sobreira, L. Avramova, R. G. Cooks and D. H. Thompson, *ACS Comb. Sci.*, 2020, **22**, 796–803.
190 D. L. Logsdon, Y. Li, T. J. Paschoal Sobreira, C. R. Ferreira, D. H. Thompson and R. G. Cooks, *Org. Process Res. Dev.*, 2020, **24**, 1647–1657.
191 G. Murbach-Oliveira, K. Banerjee, M. M. Nociari and D. H. Thompson, *ACS Bio Med Chem Au*, 2022, **2**, 297–306.
192 S. A. Biyani, Q. Qi, J. Wu, Y. Moriuchi, E. A. Larocque, H. O. Sintim and D. H. Thompson, *Org. Process Res. Dev.*, 2020, **24**, 2240–2251.
193 S. Sarkar, V. Narayanan, R. Srivastava and A. R. Kulkarni, *Ind. Eng. Chem. Res.*, 2023, **62**, 8767–8778.
194 T. T. H. Nguyen, H. K. Bui, J. Y. Im and T. S. Seo, *Small Methods*, 2025, **9**, e2400094.
195 J. Sui, J. Yan, D. Liu, K. Wang and G. Luo, *Small*, 2020, **16**, 1902828.
196 O. Długosz and M. Banach, *React. Chem. Eng.*, 2020, **5**, 1619–1641.
197 S. Bagi, S. Yuan, S. Rojas-Buzo, Y. Shao-Horn and Y. Román-Leshkov, *Green Chem.*, 2021, **23**, 9982–9991.
198 D. Senthil Raja and D.-H. Tsai, *Chem. Commun.*, 2024, **60**, 8497–8515.
199 M. H. Reis, F. A. Leibfarth and L. M. Pitet, *ACS Macro Lett.*, 2020, **9**, 123–133.
200 N. Zaquen, M. Rubens, N. Corrigan, J. Xu, P. B. Zetterlund, C. Boyer and T. Junkers, *Prog. Polym. Sci.*, 2020, **107**, 101256.

201 C. D. Jones, L. J. Kershaw Cook, D. Marquez-Gamez, K. V. Luzyanin, J. W. Steed and A. G. Slater, *J. Am. Chem. Soc.*, 2021, **143**, 7553–7565.
202 A. Seemann, J. Panten and A. Kirschning, *J. Org. Chem.*, 2021, **86**, 13924–13933.
203 F. Parveen, H. J. Morris, H. West and A. G. Slater, *J. Flow Chem.*, 2024, **14**, 23–31.
204 C. Du, A. C. Padgham, A. G. Slater and L. Zhang, *Chem*, 2025, **11**, 102328.
205 M. E. Briggs, A. G. Slater, N. Lunt, S. Jiang, M. A. Little, R. L. Greenaway, T. Hasell, C. Battilocchio, S. V. Ley and A. I. Cooper, *Chem. Commun.*, 2015, **51**, 17390–17393.
206 I. G. Clayson, D. Hewitt, M. Hutereau, T. Pope and B. Slater, *Adv. Mater.*, 2020, **32**, 2002780.
207 G. Hautier, *Comput. Mater. Sci.*, 2019, **163**, 108–116.
208 A. Jain, S. P. Ong, G. Hautier, W. Chen, W. D. Richards, S. Dacek, S. Cholia, D. Gunter, D. Skinner, G. Ceder and K. A. Persson, *APL Mater.*, 2013, **1**, 011002.
209 K. Ollerton, R. L. Greenaway and A. G. Slater, *Front. Chem.*, 2021, **9**, 774987.
210 Y. Liu, Z. Hu, Z. Suo, L. Hu, L. Feng, X. Gong, Y. Liu and J. Zhang, *Sci. China: Technol. Sci.*, 2019, **62**, 521–545.
211 N. Munyebvu, J. Nette, S. Stavrakis, P. D. Howes and A. J. deMello, *Chimia*, 2023, **77**, 312–318.
212 R. L. Greenaway and K. E. Jelfs, *ChemPlusChem*, 2020, **85**, 1813–1823.
213 M. L. Kelty, W. Morris, A. T. Gallagher, J. S. Anderson, K. A. Brown, C. A. Mirkin and T. D. Harris, *Chem. Commun.*, 2016, **52**, 7854–7857.
214 S. Baudis and M. Behl, *Macromol. Rapid Commun.*, 2022, **43**, 2100400.
215 C. J. Hampson, M. P. Smith, L. L. Arciero, C. M. Collins, L. M. Daniels, T. D. Manning, M. W. Gaultois, J. B. Claridge and M. J. Rosseinsky, *Chem. Sci.*, 2024, **15**, 2640–2647.
216 W. Zhang, M. Yu, T. Liu, M. Cong, X. Liu, H. Yang, Y. Bai, Q. Zhu, S. Zhang, H. Gu, X. Wu, Z. Zhang, Y. Wu, H. Tian, X. Li, W.-H. Zhu and A. I. Cooper, *Nat. Synth.*, 2024, **3**, 595–605.
217 M. Yu, W. Zhang, Z. Guo, Y. Wu and W. Zhu, *Angew. Chem., Int. Ed.*, 2021, **60**, 15590–15597.
218 M. O'Shaughnessy, A. C. Padgham, R. Clowes, M. A. Little, M. C. Brand, H. Qu, A. G. Slater and A. I. Cooper, *Chem.–Eur. J.*, 2023, **29**, e202302420.
219 P. R. Judzewitsch, N. Corrigan, F. Trujillo, J. Xu, G. Moad, C. J. Hawker, E. H. H. Wong and C. Boyer, *Macromolecules*, 2020, **53**, 631–639.
220 M. Rubens, J. H. Vrijsen, J. Laun and T. Junkers, *Angew. Chem., Int. Ed.*, 2019, **58**, 3183–3187.
221 B. Zhang, A. Mathoor and T. Junkers, *Angew. Chem., Int. Ed.*, 2023, **62**, e202308838.
222 L. Porwol, D. J. Kowalski, A. Henson, D.-L. Long, N. L. Bell and L. Cronin, *Angew. Chem., Int. Ed.*, 2020, **59**, 11256–11261.
223 M. B. Montaner, M. R. Penny and S. T. Hilton, *Digital Discovery*, 2023, **2**, 1797–1805.
224 A. R. Basford, S. K. Bennett, M. Xiao, L. Turcani, J. Allen, K. E. Jelfs and R. L. Greenaway, *Chem. Sci.*, 2024, **15**, 6331–6348.
225 S. Lo, S. G. Baird, J. Schrier, B. Blaiszik, N. Carson, I. Foster, A. Aguilar-Granda, S. V. Kalinin, B. Maruyama, M. Politi, H. Tran, T. D. Sparks and A. Aspuru-Guzik, *Digital Discovery*, 2024, **3**, 842–868.
226 J. R. Saugbjerg, T. B. Jensen, M. Hinge and M. L. Henriksen, *React. Chem. Eng.*, 2023, **8**, 2866–2875.